RESISTIVITY MEASUREMENT OF FERMI LIQUID COMPOUNDS

RESISTIVITY MEASUREMENT OF FERMI LIQUID COMPOUNDS

By MAHSA RAHIMI MOVASSAGH, B. Sc.

A Thesis Submitted to the School of Graduate Studies in Partial Fulfillment of the Requirements for the Degree Master of Science
September 19, 2014

MASTER OF SCIENCE (2014) (Physics and Astronomy)
McMaster University, Hamilton, Ontario
TITLE: Resistivity measurement of Fermi liquid compounds
AUTHOR: Mahsa Rahimi Movassagh, B. Sc. (Physics), Sharif University of Technology
SUPERVISOR: Dr. Thomas Timusk
NUMBER OF PAGES: xii, 70

Abstract

This thesis contains a report on resistivity measurements performed on two compounds, doped URu_2Si_2 (with Re, Fe and Rh) and Sr_2RuO_4 . These two materials are strongly correlated systems and they become superconducting at low temperature. In the first two chapters, we review Fermi liquid theory and the Kondo model. We also review some previous studies on Fermi liquid behaviour of these compounds and the hidden order phase in URu_2Si_2 (which is still not fully understood). In the following chapter we explain the resistivity measurement techniques we used and summarize the procedure of how we built the immersion probe we use in our lab at McMaster University. Finally we report the resistivity measurements on the doped URu_2Si_2 samples and Sr_2RuO_4 done in our lab and their Fermi liquid behaviour.

Acknowledgments

This thesis represents not only my work but professional and personal support of a number of people and I am using this opportunity to express my gratitude to them.
Foremost, I would like to express my sincere thanks to my supervisor Prof. Thomas Timusk for his professional and personal support, motivation and immense knowledge since the day I joined his group and also for his guidance and help and patience throughout the writing of my thesis. I also would like to acknowledge Ph.D. candidates Jesse Hall and Nathan Armstrong and M.Sc. candidate Kevin Mortimer for helpful discussions and assistance. I should also extend my thanks to Kevin Mortimer for growing and providing the Sr_2RuO_4 sample with the technical assitance of Prof Maeno and his group at Kyoto University for our experiments.

Next, I would like to thank Prof Graeme Luke who provided me with valuable information on resistivity measurement techniques, shared his lab space and equipment. Thanks also go to Dr. Paul Dube for technical assistance, keeping a steady supply of Liquid Helium, for resistivity measurements and for help in building the immersion probe. Marek Kiela and Dr. Antoni Dabkowski also assisted us in building the immersion probe.

I should also thank Prof. Matsuda at Kyoto University for providing the URu_2Si_2 resistivity and first derivative data. I should also acknowledge Prof. Maple at the University of California, San Diego for providing us with $URu_{2-x}Re_xSi_2$ (with $x = 0.02$, 0.07 and 0.1) and $URu_{2-x}Fe_xSi_2$ (with $x = 0.1$), Dr. Travis Williams a former PhD candidate and Murray Wilson a current PhD candidate of Prof. Graeme Luke's group for crystal growth of $URu_{2-x}Rh_xSi_2$ (with $x = 0.04$) and $URu_{2-x}Fe_xSi_2$ (with $x = 0.2$ and 0.3). In addition, I would like to express my thanks to Prof. Stephen Julian and his PhD student Di Tian at the University of Toronto for helping us with making resistivity contacts.

Lastly, special thanks to my wonderful family for all their support through my studies.

Contents

List of Figures

List of Tables

Chapter 1

Introduction

Fermi liquid compounds are metallic materials that are characterized by an electrical resistivity that varies as $(k_B T)^2$ at low temperatures where T is the absolute temperature. Theory shows that the resistivity should also vary with frequency as $(\hbar\omega)^2$ and the scaling between the two terms is a dimensionless constant $4\pi^2$. It was shown recently by Nagel *et al.* [2] that for a large selection of materials this simple rule is not obeyed. It was therefore important to study other materials to investigate the systematics of this phenomenon. One aspect of such an experimental program is an accurate measurement of the temperature dependence of the electrical resistivity. The purpose of this thesis is to develop methods for resistivity measurements and test these on a variety of Fermi liquid compounds.

The thesis is organized as follows. First we give some background on Fermi liquid theory as it applies to the optical conductivity and the scaling between temperature and frequency dependence. Then we discuss the two families of compounds we used to test our experimental methods. The first system is the heavy fermion compound URu_2Si_2 doped with Re, Fe and Rh, where in the undoped materials, anomalous Fermi liquid scaling was first observed by Nagel *et al.*[2]. The second material is Sr_2RuO_4 a compound that is well studied by both angle resolved photo emission and quantum oscillations. There is general agreement in the field that its Fermi surface, while highly anisotropic, is well understood. It is supposed to be a canonical Fermi liquid and if that is the case, it should follow the $4\pi^2$ scaling law. In the following section we discuss experimental methods of measuring resistivity and the method used in the thesis. Then we turn to the actual results obtained and an analysis of the data in terms of power laws in temperature. Finally we close by drawing some conclusions.

Chapter 2

Fermi liquid theory

The transport properties of electrons in metals were first explained by Drude in 1900. The so-called Drude model is based on classical mechanics and assumes that a metallic environment consists of relatively stationary ions in a sea of free electrons. Drude constructed his model based on the following assumptions:
1- The interaction between electrons is neglected.
2- The only interaction of the free electrons with the ions is due the instantaneous collision which abruptly changes the velocity of an electron.
3- τ is the average time between two successive collisions which is also known as mean free time or relaxation time.
4- The electrons finally reach thermal equilibrium with their environment due to the collisions.

Based on the above assumptions, an applied electric field causes the electrons to accelerate but stop when they collide with ions due to the electostatic force. Therefore, instead of reaching infinite velocity, electrons travel through their surrounding with an average or drift velocity $\vec{v}$.

Drude showed that the drift velocity and τ are related by:

$$\frac{d\vec{v}}{dt} = -\frac{e\vec{E}}{m} - \frac{\vec{v}}{\tau} \tag{2.0.1}$$

where e is the electron charge, $\vec{E}$ the electric field and m is the mass of the electron.

Later, in the 1930's, Sommerfeld developed the so called Fermi gas model for metals based on quantum mechanics. In this model electrons are considered as non interacting fermions which obey Fermi-Dirac statics and follow the

Pauli exclusion principle. They fill the electronic states with energy $\frac{\hbar^2}{2m}k^2$ in k space. The highest occupied momentum state is the Fermi momentum k_F and the energy associated with it $\frac{\hbar^2}{2m}{k_F}^2$ is the Fermi energy. In the Sommerfeld model an electron is described by a wave function which satisfies Schrödinger's equation.

However, in a real metallic environment, all the particles interact with each other and sometimes the interaction is so strong that it cannot be neglected. Therefore, in a real condensed matter system we have to deal with a large number of particles (10^{23} particles/cm^3) which interact. There is no general solution of the Hamiltonian of this many body system but various approximate solutions have been developed. One of these approximate approaches, which is successfully able to treat many body problems at low temperature, is the phenomenological Landau Fermi liquid theory introduced by Landau in 1957. In this theory the interacting fermions are approximated by noninteracting quasi particles.

In his theory, Landau started with a non-interacting Fermi gas. Then the interactions are adiabatically turned on and as a result the spin, momentum and charge of the particles in k states remained unaffected but their mass, magnetic moment and other dynamic properties are changed and renormalized and therefore the energy of the system is changed too. This new system is called a Fermi liquid and the elementary excitations associated with it are called quasi particles. There is a one to one correspondence between these quasi particle of the Fermi liquid system and elementary excitations of the non-interacting Fermi gas, called Landau quasi particles that decay with a lifetime $\tau \propto \frac{1}{(E-E_F)^2}$ at low T where E is the energy of a quasi particle.

Based on Fermi liquid theory, in 1959 Gurzhi [11] showed that the resistivity of a metal is given by

$$\rho(\omega, T) = A((\hbar\omega)^2 + 4(\pi k_B T)^2) \tag{2.0.2}$$

where ω is the frequency of the alternating electric field applied to the metal and T the absolute temperature.

Recently, Malsov and Chubukov [12] derived a more general relation for frequency dependent resistivity:

$$\rho(\omega, T) = A((\hbar\omega)^2 + b(\pi k_B T)^2) \tag{2.0.3}$$

where the coefficient $b = 4$ for the conventional electron-electron umklapp scattering of a Fermi liquid in accord with Gurzhi's formula, but for elastic resonant scattering $b = 1$. The value of $b = 1$ is in fact observed in many strongly correlated systems [2]. For mixed system of umklapp and resonant scattering b can take on intermediate values.

Chapter 3

Kondo model and heavy fermion systems

3.1 Introduction

The first heavy fermion compound $CeAl_3$ was discovered by Andres *et al.*[13] in 1975. They observed a very large specific heat coefficient γ in this compound at low temperature as compared to ordinary metals.

The specific heat of normal metals consists of an electron and a phonon contribution, where at low temperature, the electronic specific heat is dominant and is proportional to the electron effective mass [13].

$$C = C_e + C_{ph} = \gamma T + AT^3 \tag{3.1.1}$$

Therefore, the extremely large γ ratio observed in $CeAl_3$ indicates that the effective mass is about 1000 times larger than the free electron mass.

In fact, the interesting properties of heavy fermions come from the electrons in partially filled f orbitals of these atoms. At room temperature the f orbital electrons are localized and act like independent spins. But at low enough temperatures, the f electrons interact with the conduction elections, leading to antiferromagnetic (AFM) ordering or extremely large effective electron masses [14], see Figure 3.1.

Hence, we cannot use the free electron model to describe heavy fermions at low temperature. The successful many-body model which can describe heavy fermion behaviour is the lattice Kondo model, also called the Anderson model.

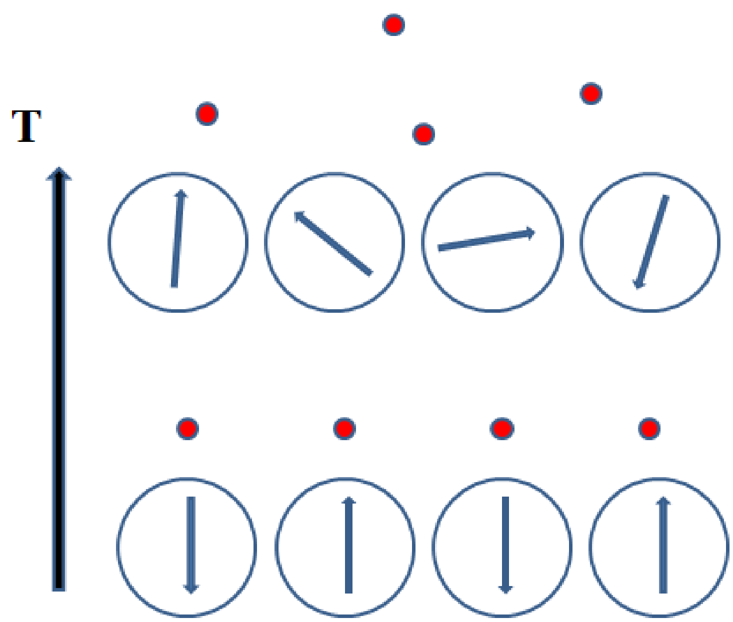

Figure 3.1: The blue arrows show the electrons in f orbitals of the atoms (large blue circles) in a heavy fermion compound. At high temperature, the f electrons are localized and do not interact with the f electrons on the neighboring atoms or conduction electrons (red dots). At low temperature the f electrons at different atoms are correlated and coupled to the conduction electrons.

This model is a lattice version of the model originally proposed by Kondo [15] to describe the minimum resistivity observed in metals containing magnetic impurities and will be discussed in the following section.

3.2 The Kondo model and the Kondo effect

In an attempt to give a picture that describes heavy fermion systems at low temperature, we should start with the problem of the Kondo effect.

In normal metals, at low temperature, the electrical resistivity drops monotonically to finally flatten out and become temperature independent. The temperature independent part is a signature of the process of elastic scattering from static impurities. However in early 1930 a minimum resistance was observed in metals at low temperature and it took over 30 years to realize that this effect is related to the magnetic moments of the impurities. The minimum resistance observed in metals with very dilute magnetic ions is called the Kondo effect and it happens below characteristic temperature T_K [16].

This effect is due to the fact that the impurity magnetic moments become screened by free conduction electrons with opposite spin-polarization and together form a quasi-bound state. At low temperature they make non-magnetic resonant scattering centers for conduction electrons in the Fermi sea. In other words, the increase in resistivity is due to the impurity magnetic moments which form a strong elastic scattering potential for conduction electrons [14] (Figure 3.2).

The first attempt to develop a model to understand the microscopic mechanism of the Kondo effect was by Anderson who proposed a model Hamiltonian which describes the formation of magnetic moments in metals [17]:

$$H = \sum_{i\sigma} \varepsilon_f n^f_{i\sigma} + V \sum_{i\sigma} (c^\dagger_{i\sigma} f_{i\sigma} + f^\dagger_{i\sigma} c_{i\sigma}) + E_f n_f + U n^f_{i\downarrow} n^f_{i\uparrow} \tag{3.2.1}$$

where σ denotes the spin of the electrons, $c_{i\sigma}$ and $f_{i\sigma}$ are conduction and local f orbital electron operators. The first term describes the isolated localized f electron, then second and third terms indicate the hybridization of orbitals and coulomb interaction between the electrons in the f orbitals. The above Hamiltonian is called the single impurity Anderson model.

Anderson argued that if U, the coulomb interaction, is much larger than

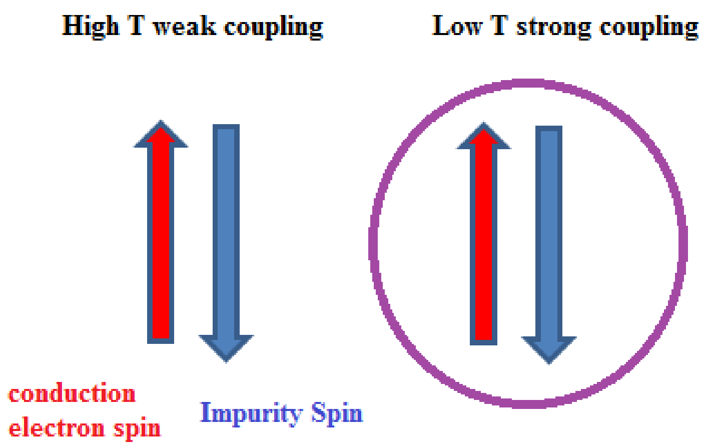

Figure 3.2: Schematic Kondo effect formation

the kinetic energy of the f electrons, local magnetic moments form and the Kondo effect appears. This means that in each f orbital we can only have one electron and this state is called the Kondo regime. [17]

By using the second order of perturbation with respect to V we can obtain an effective Hamiltonian which is called the Kondo model:

$$H_{\mathrm{K}} = \sum_{i\sigma} \varepsilon_f n_{i\sigma}^f + J \sum_{i\sigma} S_i . S_i^c \tag{3.2.2}$$

where J is the exchange interaction of conduction and localized impurities spins and is given by $8V^2/U$. Based on this Hamilton, Kondo derived the logarithmic part of the resistivity which explains the Kondo effect. [18]

3.3 The Kondo model and heavy fermions

After the discovery of heavy fermions, Doniach [19] suggested that heavy fermion systems form a dense Kondo lattice where every local moment in the lattice experiences the Kondo effect. This is due to the fact that the f electrons mobility is very small so, heavy fermion materials are in the Kondo regime.

In addition, the local moments also interact with each other via indirect RKKY exchange interaction which, if it strong enough, can cause an antiferromagnetic ordered state.

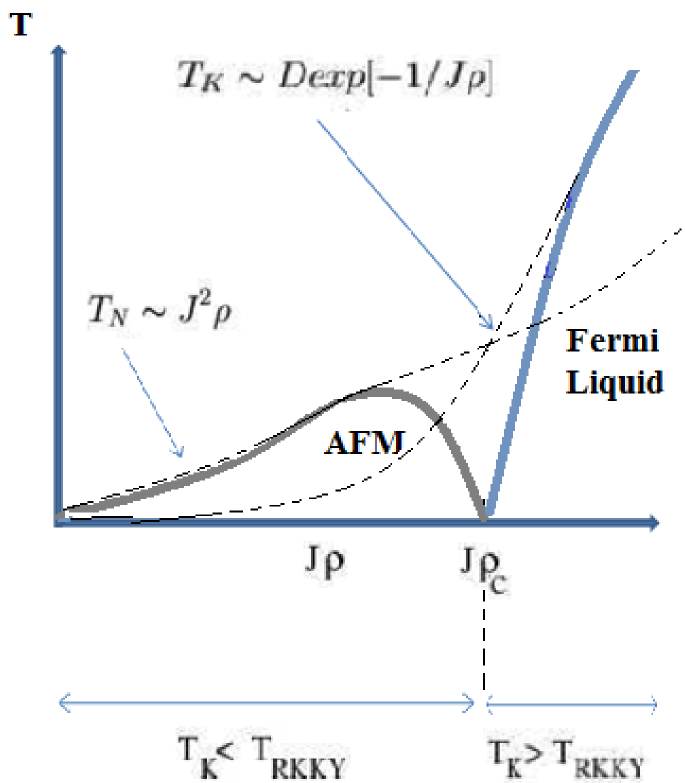

Figure 3.3: Doniach diagram, showing that the Fermi liquid regime (heavy fermion regime) and the antiferromagnetic regime meet at a quantum critical point, $J\rho_c$; the dashed lines show the effective Kondo and RKKY temperatures. They cross at the quantum critical point.

Doniach argued there is a competition between the Kondo effect with Kondo temperature $T_{\mathrm{K}} \propto De^{-1/(J\rho)}$ and an antiferromagnetic state with Néel temperature $T_{\mathrm{N}} \propto J^2\rho$. This is shown in Figure 3.3

He compared these two different temperatures and found that when J is small, RKKY interaction becomes dominant and T_{RKKY} is the largest energy scale so, local moments are strongly correlated and the system is ordered in an antiferromagnetic state. On the other hand, when J is large, T_{K} is large and the RKKY interaction is not important and the ground state is a dense Kondo lattice state. Each local spin forms a singlet state with a conduction electron to form a paramagnetic state [19].

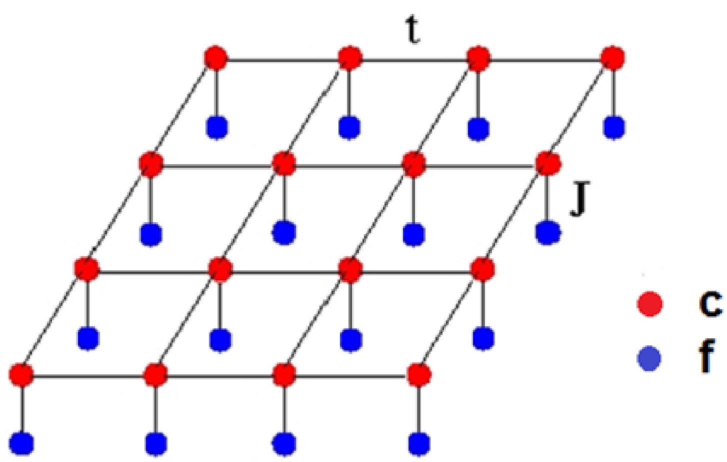

Figure 3.4: Two-dimensional lattice for heavy fermions. Red balls represent conduction electrons where they interact with f orbital electrons (blue balls)

Chapter 4

Two Fermi liquids: doped URu_2Si_2 and $Sr_2(Ru,Rh)O_4$

Uranium-based compounds have attracted wide interest since the discovery of heavy fermion behaviour and superconductivity in UPt_3 by Stewart *et al.* [20] and UBe_{13} by Ott *et al.* [21]. Some of the U-based compounds have shown an interesting competition between superconductivity and magnetism. These behaviours are related to the properties of the electrons in unfilled 5f orbitals. These compounds can be characterized as heavy fermion Fermi liquids but under some circumstance also as non Fermi liquids. One of these materials, which has been studied for more than two decades, and whose puzzling characteristics are not fully understood yet, is URu_2Si_2 [22].

Palstra *et al.* [23] were first to observe *two* phase transitions in the heavy fermion compound URu_2Si_2. One is the superconducting transitions which occurs at ~ 1.0 K, and, which after about 30 years since its discovery has been recently identified as an unconventional d-wave superconductor with time reversal symmetry breaking [24]. The other transition appears at ~ 17.5 K and was interpreted initially [23, 25, 26] in terms of various magnetic states such as a spin density wave state, itinerant antiferromagnetism or local U moment antiferromagnetism. However neutron scattering experiments showed little evidence of the substantial ordered moment expected for these states. Long range order magnetism or spin density wave formation are now thought to not be responsible for the phase transition at 17.5 K. Since the order parameter and elementary excitations of this phase transition are still unknown, 25 years after its discovery, this mysterious transition is called the hidden order (HO)

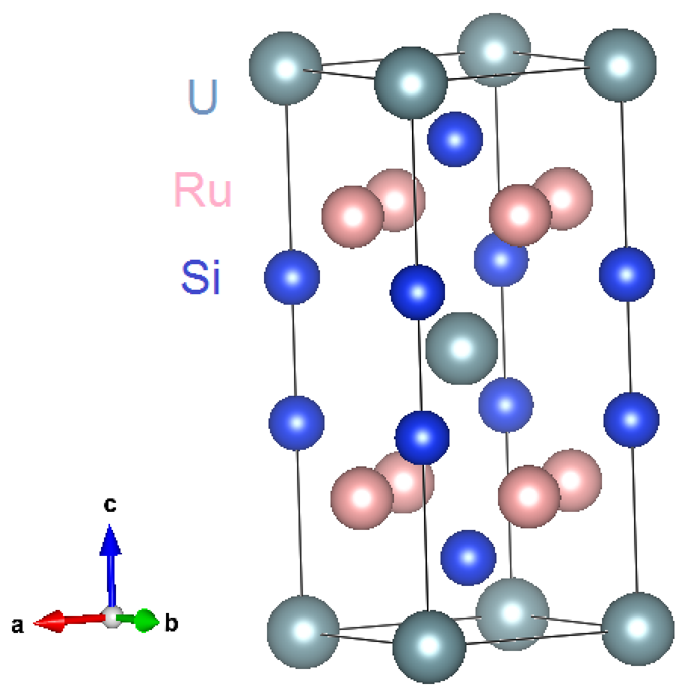

Figure 4.1: Crystal structure of URu_2Si_2: body centered tetragonal with space group $I4/mmm$

transition.

4.1 Hidden Order

The HO transition is a second order phase transition (detected by bulk quantities such as specific heat) where the entropy of the system is reduced significantly on going into the HO phase. Another characteristic of this phase are that the quasi particles effective mass is found to increase substantially [27] at the transition and that pressure, magnetic field and Rh doping can destroy it. The superconducting temperature and resistivity is dependent on the quality of the sample and they become smaller with increasing purity of sample [3]. However, T_{HO} is less sensitive to sample purity and occurs at 17.5 K in most reports on undoped samples. [22]

4.2 Resistivity measurement of URu_2Si_2

One of the important ways to study the HO phase is through transport measurements. In the early studies of URu_2Si_2, transport measurements showed that the Fermi surface is reconstructed at the HO phase transition [23], [26]). Maple *et al.* [23] and Fisher *et al.* [28] showed that the electronic specific heat C_e in the HO state is given by $C_e \propto exp(-\Delta/k_B T)$ where Δ is the gap. The fits of the data gave $\Delta = 11$ meV and was found to open over about 40% of the Fermi surface (Palstra *et al.* [23], Maple *et al.* [26]). In addition, the HO transition is visible as a jump in the electrical resistivity. In 1987, McElfresh *et al.* calculated a gap of 7 meV from resistivity measurement [29].

Here we focus on resistivity measurements to study the characteristics of URu_2Si_2. The resistivity of URu_2Si_2 along the a axis is displayed in Figure 4.2 [1]. The resistivity above 100 K increases as the temperature decreases down to $\sim$ 70 K, typical of Kondo impurity behaviour. In this region (above 100 K) the localized f electrons act like isolated magnetic impurities giving rise to incoherent scattering which increases as the temperature is lowered. The localized spins start to be screened out by conduction electrons at around 70 K and the heavy fermion state starts to form. As the f electrons hybridize with the conduction electrons the local U spin scattering decreases and the resistivity drops with decreasing the temperature. Near the hidden order

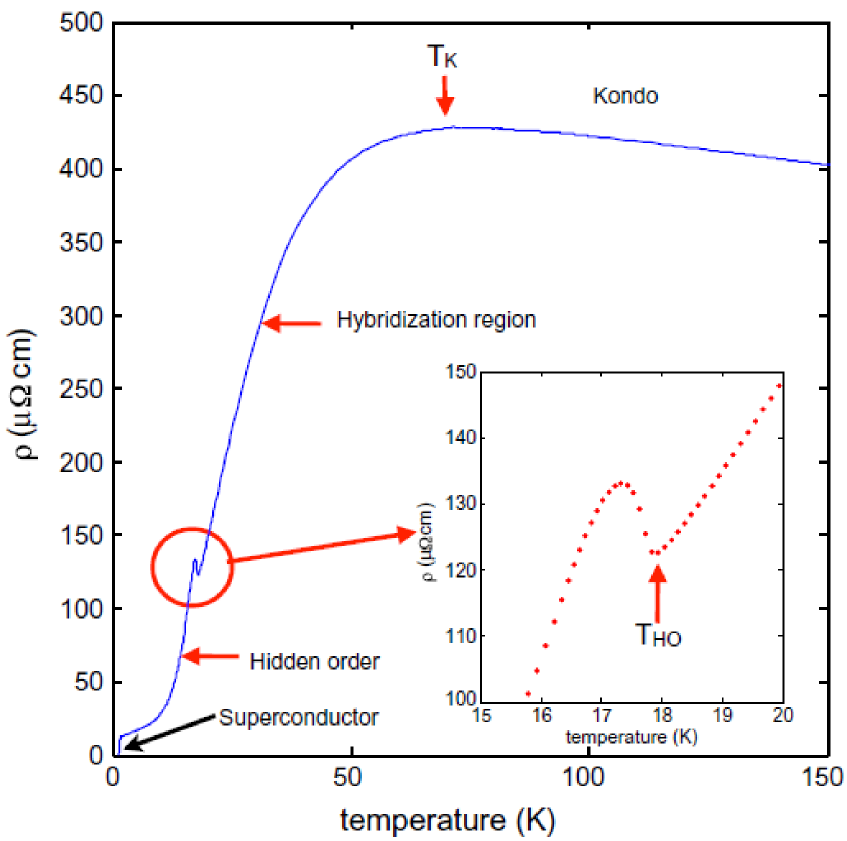

Figure 4.2: The resistivity of URu_2Si_2 as a function of T; different states and transitions described in the text are shown here. The inset is ρ around HO phase transition (reprinted from [1])

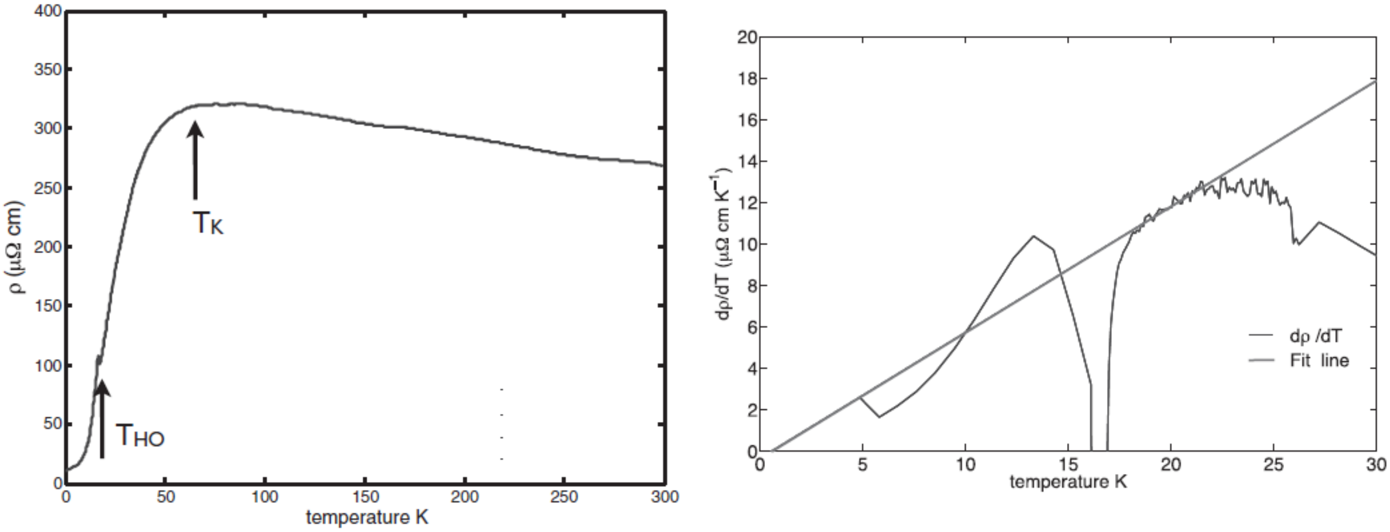

Figure 4.3: The plot on the left shows the inter-plane resistivity of URu_2Si_2. On the right, the solid curve represents $d\rho/dT$ of URu_2Si_2. The straight line is the Fermi Liquid fit in the temperature range 18–22 K using equation $d\rho/dT = 2AT + B$, (reprinted from [2]) .Copyright 2012 by Proceedings of the National Academy of Sciences of the United States of America, PNAS

transition the system is Fermi liquid, although with an anomalous scaling between the temperature and frequency dependences [2]. As we lower the temperature further, below the hidden order transition at 17.5 K, we observe a slight increase in resistivity. This increase is due to the formation of gap over a a considerable part of the Fermi surface which causes a loss of carriers. The region in which the FS is gapped is the called gapped Fermi liquid region. As the gap forms, a competing process takes over (there are fewer final states to scatter to) and the resistivity begins to decrease as the temperature is lowered to finally enter the superconducting state at about 1.5 K [1].

The Fermi liquid behaviour of URu_2Si_2 has been studied by different groups [2, 30, 24]. The resistivity of a sample of URu_2Si_2 as a function of T is shown in Figure 4.3 (left). In the right hand panel the derivative of the Fermi liquid equation $d\rho/dT = 2AT + B$ was fitted to the measured resistivity derivative in the temperature range 18-22 K which gave $A = 0.3 \pm 0.12\mu\Omega\text{cm K}^{-2}$ [2],. The coefficient $B = 0$ to within experimental error.

The sensitivity of the HO and the superconducting transition temperatures to sample quality has been investigated by Matsuda *et al.*[3]. They have

Table 4.1: The fit coefficients of equation 4.2.1 for URu_2Si_2 in the HO state (from [3])

	$\rho_0(\mu\Omega.cm)$	$A(\mu\Omega.cmK^{-2})$	$B(\mu\Omega.cmK^{-2})$	$\Delta(K)$
$J \parallel a-axis$	1.05	0.099	259	76.4

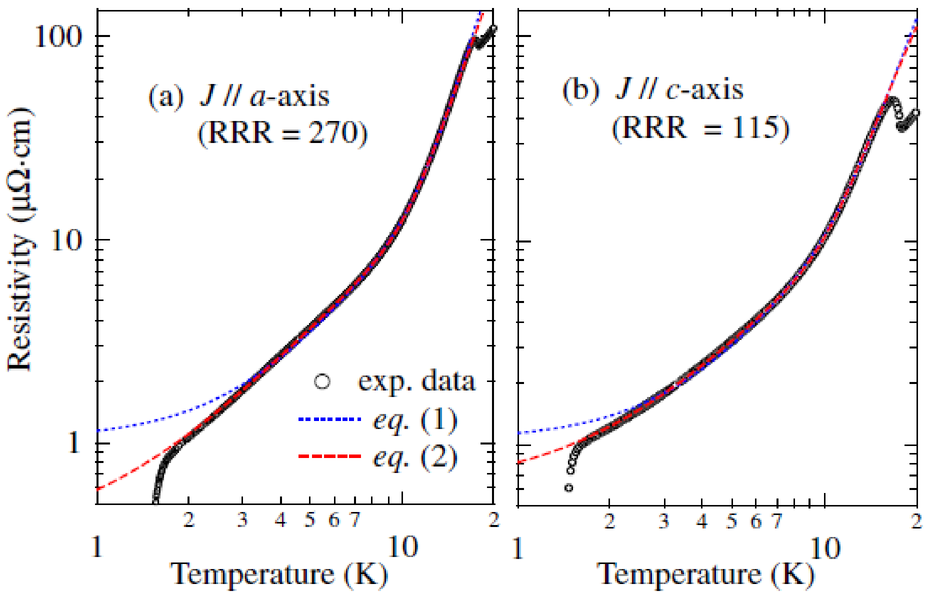

Figure 4.4: The low temperature resistivity of URu_2Si_2 vs. T along (a) a and (b) c direction, the dashed lines show the curves fit using the formula 4.2.1 (eq.(1)) and 4.2.2 (eq. (2)) (reprinted with permission from [3]) Copyrighted by the Physical Society of Japan.

measured and compared the resistivity and specific heat data of different samples cut from different parts of a single crystal. They observed that for samples with residual resistivity ratios, RRR > 50, $T_{\rm HO}$ and $T_{\rm SC}$ are independent of RRR [3]. The resistivity in the HO state (gapped Fermi Liquid region) has also been studied by Matsuda *et al.* using equation 4.2.1 [3].

$$\rho(T) = \rho_0 + AT^2 + BT(1 + \frac{2T}{\Delta})exp(-\frac{\Delta}{T}) \tag{4.2.1}$$

Using the equation 4.2.1, the best fit parameters are summarized in table 4.1 for the temperature range between 2–15 K.

As discussed above, equation 4.2.1 is derived for gapped spin waves in an antiferromagentic system and there is no justification to apply it to the HO

Table 4.2: The fit coefficients of equation 4.2.2 for URu_2Si_2 in the HO state (from [3])

	$\rho_0(\mu\Omega.cm)$	$A(\mu\Omega.cmK^{-2})$	$B(\mu\Omega.cmK^{-2})$	$\Delta(K)$	x
$J \parallel a-axis$	0.32	0.26	10800	85	1.58

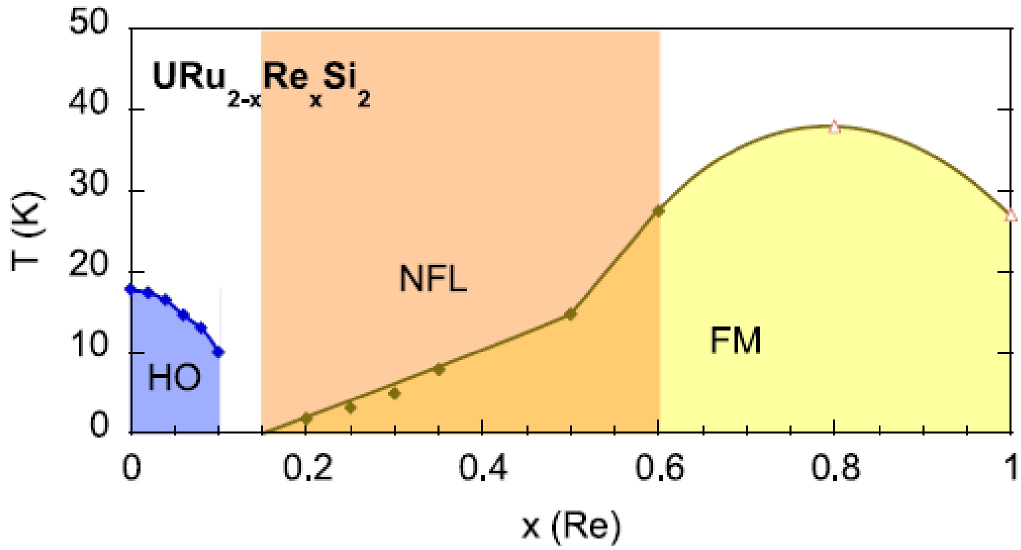

Figure 4.5: The phase diagram T vs. x of $URu_{2-x}Re_xSi_2$ (reprinted with permission from Butch *et al.*[4]). Copyright 2010 by Institute of Physics

state in URu_2Si_2 [3]. As Figure 4.4 shows, the gapped Fermi liquid equation 4.2.1 deviates considerably at low temperature. Therefore, it is believed that the HO region should not simply be considered to be a Fermi liquid with an open gap and its behaviour is more complicated. Instead a better fit is achieved by applying the phenomenological expression from Matsuda *et al.* [3]:

$$\rho(T) = \rho_0 + AT^x + BTexp(-\frac{\Delta}{T}) \tag{4.2.2}$$

The best fit parameters are shown in table 4.2 which indicates that x is different from 2 and for the same temperature range formula 4.2.2 is a better fit (table 4.2).

4.2.1 Re doped URu_2Si_2

One of the ways to investigate the robustness of a system is chemical substitution or doping, the replacement a small fraction of one of the three elements of URu_2Si_2 and the effect of such substitutions on the properties of the HO phase. Replacing U with Th or other rare earths has shown the quick suppression of the HO phase transition temperature while substitution of Si does not show any noticeable effect, which indicates the crucial function of U f electrons in the formation of the HO phase[4].

The Ru atom has been substituted with different elements such as Mn, Th, Fe, Os, Ir and Re. All these elements suppress the HO order transition at 5 % substitution except for Os. Rh and Fe induce antiferromagnetic phases with larger moments than the hidden order phase. In addition, a complex magnetic structure arises at intermediate Rh doping where the HO phase is transformed into the large moment AF phase [4].

An interesting chemical substitution is Re which slowly reduces the HO order parameter to zero and puts the system into a ferromagnetic (FM) phase where the transport properties show non Fermi liquid (NFL) behaviour. The NFL is characterized by anomalous power laws of the various physical properties such as specific heat and electrical resistivity. For example, the resistivity is given by $\rho(T) \propto T^x$ where $x < 2$ (where $x = 2$ is the value expected from Fermi liquid theory).

A recent study of $URu_{2-x}Re_xSi_2$ was done by the Maple group[4]. Their results on the specific heat and electrical resistivity for $0.0 \leq x \leq 0.10$ are summarized in Figure 4.6. The hidden order phase transition, can be identified as a small peak in the resistivity at T_{HO}. The HO transition can also be seen as a large peak in the specific heat (depicted in Figure 4.6 (b)) which can be interpreted in terms of a partially gapped Fermi surface. With increasing x, T_{HO} decreases and the peak in $\rho(T)$ and the anomalies in C_v are broadened and less visible. The hidden order transition can not be detected for $x = 0.12$.

4.2.2 Fe doped URu_2Si_2

Another interesting substitution for Ru that gives us information about the electronic ground state of URu_2Si_2 is iron. The effect of iron doping in URu_2Si_2 on the electrical resistivity was measured by Kanchanavatee *et al.*[5]. URu_2Si_2 and UFe_2Si_2 have the same crystal structure ($I4/mmm$). However, by increasing the amount of Fe the lattice parameter a decreases. Therefore the volume of unit cell $URu_{2-x}Fe_xSi_2$ decreases with x. This is based on the fact that Fe ions are smaller than Ru ions. Thus iron substitution can be looked on as applying chemical pressure to the material. It is known that physical pressure on URu_2Si_2 causes the material to turn into the large moment antiferromagnetic (LMAF) phase [31]. It is not clear at what Fe concentration this transition occurs and resistivity measurements cannot distinguish between HO and LMAF phases since the electronic structure changes very little across this phase transition [32]. We will call the Fe induced phase HO/LMAF phase.

The electrical resistivity, specific heat and magnetization of $URu_{2-x}Fe_xSi_2$ with different x have been measured by Kanchanavatee *et al.* [5]. In Figure 4.7 the HO/LMAF temperature is indicated by $T_0(x)$ and it is observed as a small kink in $\rho(T)$ or a sharp minimum in $d\rho(T)/dT$. As x increases from 0 to 0.8, $T_0(x)$ increases linearly from 17.5 K to its maximum value of 42 K. For $x > 0.8$ $T_0(x)$ starts to decrease and has completely disappeared at $x = 1.3$. In addition, the kink in $\rho(T)$ at $T_0(x)$ starts to broaden considerably with increasing x.

To characterize the HO/LMAFM phase, fits of a theoretical model, equation 4.2.1, have been carried out on $\rho(T)$ and they describe the data in the HO/LMAFM very well. However, as discussed by Maple *et al.*, since equation 4.2.1 was derived to explain ferromagnetic magnons and since in URu_2Si_2 the magnons detected are antiferromagnetic, a better expression for the gapped part of electrical resistivity is:

$$\rho(T) = \rho_0 + AT^x + B\Delta^2\sqrt{\frac{T}{\Delta}}[1 + \frac{2}{3}\frac{T}{\Delta} + \frac{2}{15}(\frac{T}{\Delta})^2]exp(-\frac{\Delta}{T}) \qquad (4.2.3)$$

The differences between fit parameters calculated using equations 4.2.1 and 4.2.3 are not significant since the dominant term in both is $exp(-\frac{\Delta}{T})$. In addition, the gap has been calculated from the measured specific heat. The specific heat

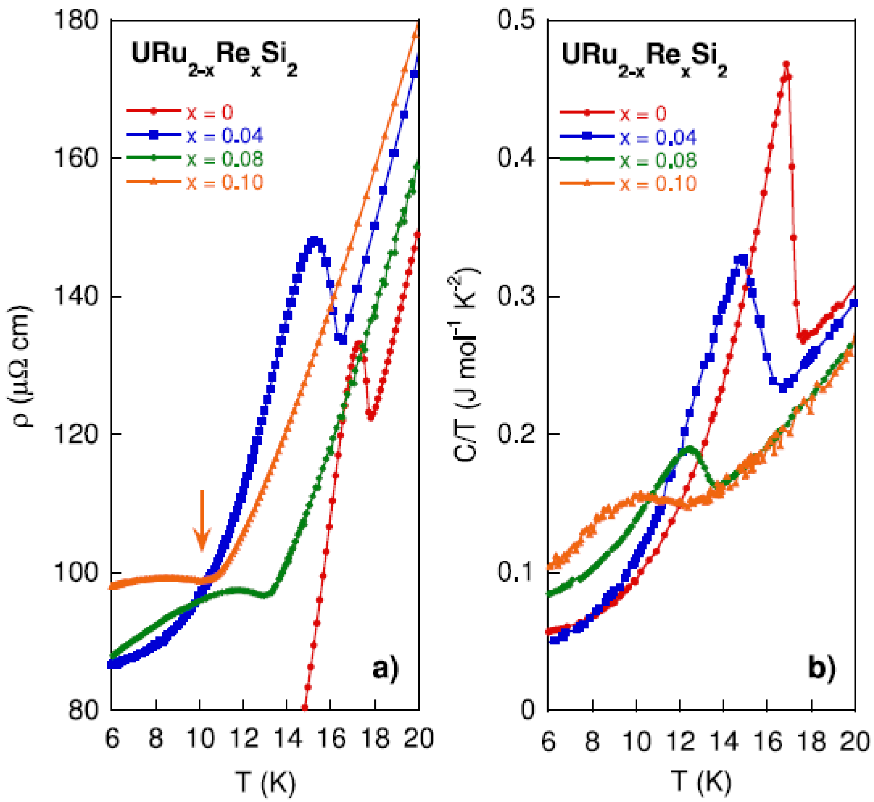

Figure 4.6: Resistivity and specific heat anomalies of $URu_{2-x}Re_xSi_2$ around HO transition. (a) T_{HO} with increasing Re doping (x) (b) The jump in the heat capacity gets smaller and broadens with increasing x (reprinted from [4]). Copyright 2010 by Institute of Physics

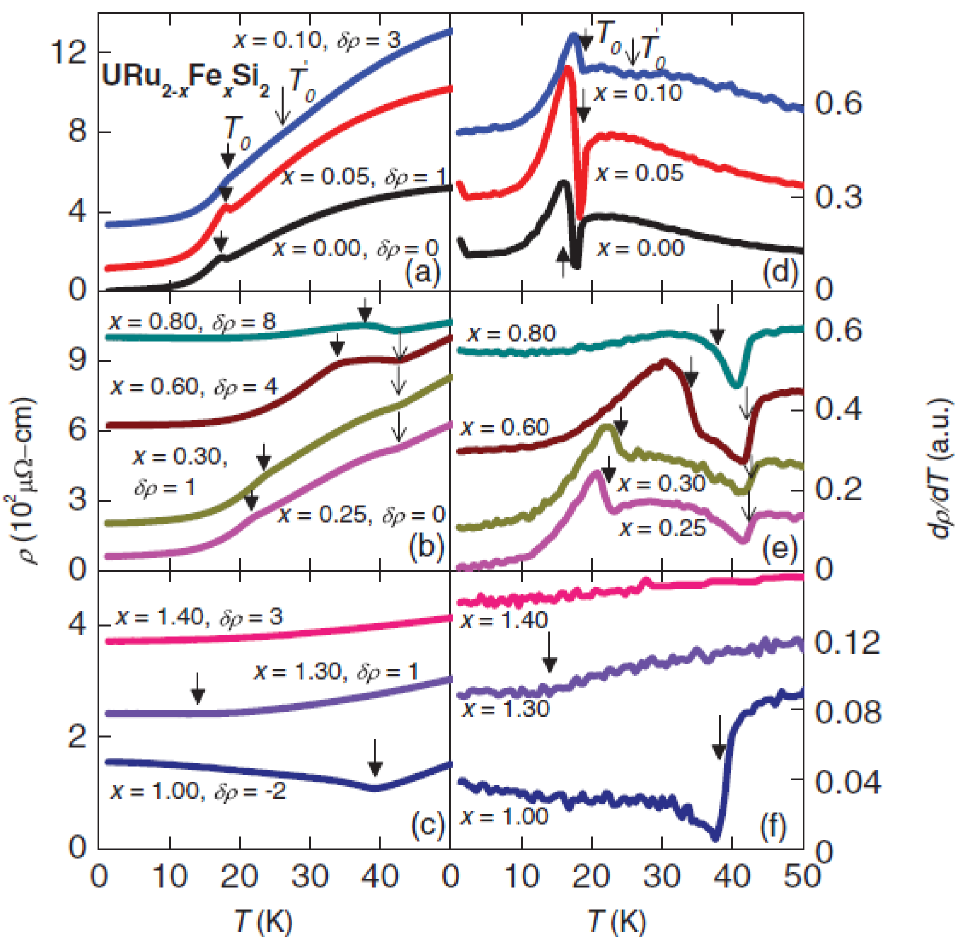

Figure 4.7: (a)-(c) the resistivitiy of $URu_{2-x}Fe_xSi_2$ as a funcntion of T near the HO/LMAFM transition for different x values (each data set is shifted by different $\delta\rho$ values). (d)-(f) The first derivative of resistivity with respect to T: $d\rho/dT$ (the HO/LMAFM transition temperature is indicated by a dark arrow) (reprinted from [5]). Copyright 2011 by the American Physical Society.

is described below T_{HO} [5] by:

$$C_e(T) = Aexp(-\frac{\Delta}{T}) \tag{4.2.4}$$

Figure 4.8 shows that the gap increases with increasing amount of Fe doping and reaches its maximum at $x = 0.1$. The figure also shows γ/γ_{e^-}, the ratio of the measured specific heat to the calculated one with a free electron mass. The ratio is shown for T below the HO/LMAFM transition and above $T_{HO/LMAFM}$, in the ungapped state. This ratio can give an estimate of the fraction of the Fermi surface which is gapped. The ratio γ/γ_{e^-} is calculated for different values of x. The data at $x = 0.0$ showing that 55% of the Fermi surface is gapped is in agreement with earlier results [26]. The γ/γ_{e^-} ratio increases with increasing x which results to increase the fraction of FS which is gapped. This fraction reaches its maximum of 80%. The results also show that the gap values calculated from 4.2.3 match with the gap values extracted from low temperature C_v fits.

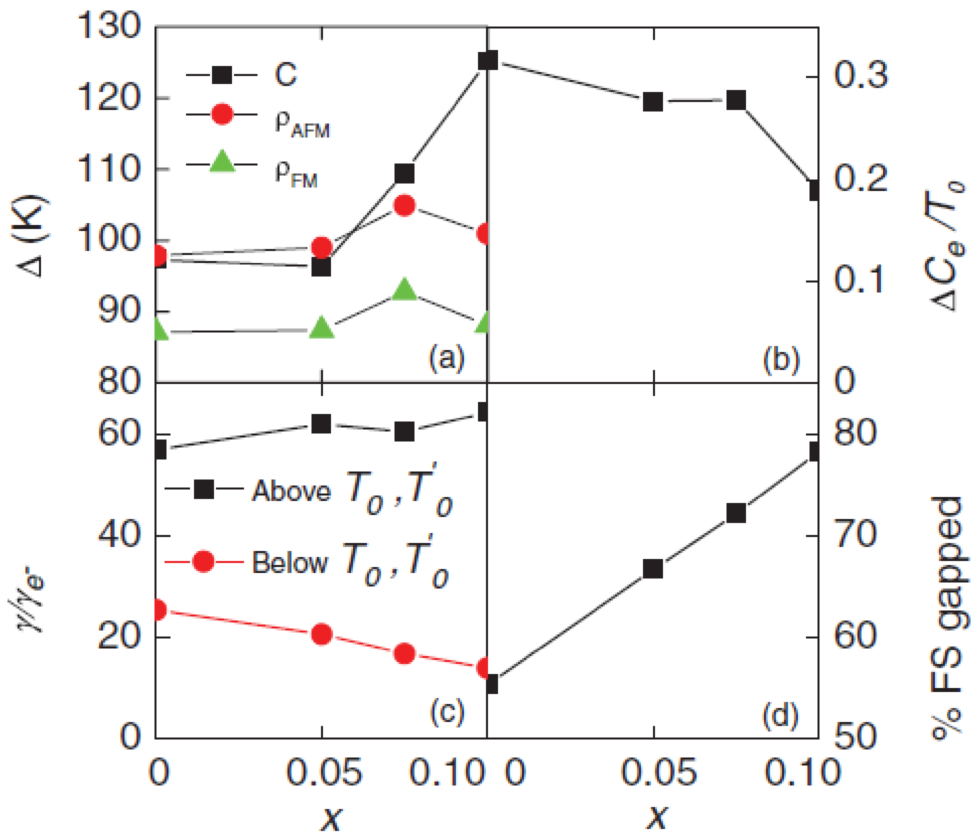

Figure 4.8: (a) Energy gap of $URu_{2-x}Fe_xSi_2$ for different x values calculated from fits using equations 4.2.3 (red circles) and 4.2.1 (green triangles), (b) The ratio of the jump of the electronic specific heat ΔC_e to HO/—MAFM temperature vs. x, (c) γ/γ_{e^-} vs. x, (d) The fraction of Fermi Surface gapped vs. various Fe concentrations x in the HO/LMAFM phase (reprinted from [5]). Copyright 2011 by the American Physical Society

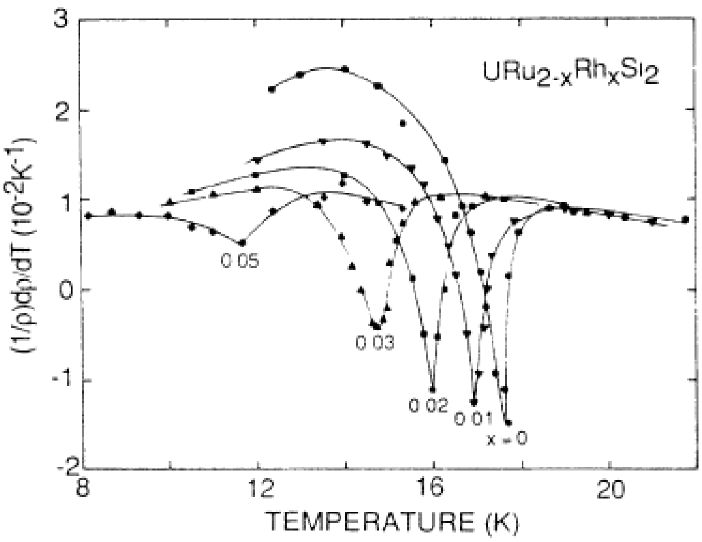

Figure 4.9: The ratio $(1/\rho)(d\rho/dT)$ for $URu_{2-x}Rh_xSi_2$ for different Rh concentrations vs T. The HO transition emerges as the minimum of the function $(1/\rho)(d\rho/dT)$ and it gets smaller with increasing x, T_{HO} is suppressed with x as well (reprinted from [6]). Copyright 1990 by the American Physical Society

4.2.3 Rh doped URu_2Si_2

Rhodium doping suppresses the hidden order temperature in $URu_{2-x}Rh_xSi_2$ gradually and at $x = 0.08$ the HO state, which appears as the minimum in the ratio $(1/\rho)(d\rho/dT)$, is destroyed and is replaced by an antiferromagntic state. Figure 4.9 shows the effect of Rh concentration on HO transition studied by Dalichaouch *et al.*[6].

4.3 Sr_2RuO_4

Sr_2RuO_4 is a moderately heavy fermion system with a specific heat coefficient γ of 3.6 due to strong correlation between Ru $4d$ electrons and oxygen p electrons. The superconductivity in Sr_2RuO_4 was first discovered by Maeno *et al.* in 1994 [7], however, this compound itself has been known since the 1950's. (High quality samples of this material become superconducting at ~ 1.5K).

The superconducting transition temperature of Sr_2RuO_4 is very low but the discovery was remarkable and generated lots of interest in this material due to its

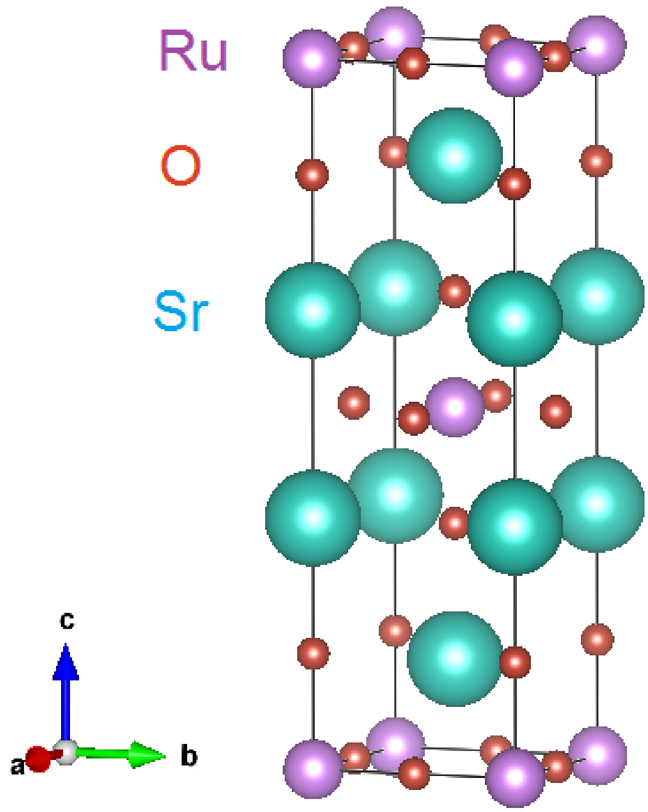

Figure 4.10: The crystal structure of Sr_2RuO_4 with tetragonal axes a, b, c

structural similarities to the high temperature superconductor $La_{2-x}Sr_xCuO_4$ and therefore raising hopes of finding an analogue system to the high T_c cuprates. The two materials have almost identical crystal structures and are quasi-two dimensional. However, Sr_2RuO_4 has metallic behaviour without doping and unlike the cuprates it becomes superconducting only at very low temperature. In that sense it is more like the uranium based heavy fermion materials.

The Maeno group performed resistivity measurements both in ab plane and c direction. They found the material to be highly anisotropic, a good metal in the ab plane, but exhibiting a heavy fermion like resistivity in the c direction, first rising to a maximum as the temperature is lowered, and then showing a Fermi liquid like behaviour to the lowest temperatures in agreement with an early study by Lichtenberg *et al.*[33]. This is shown in Figure 4.11. They observed a superconducting transition of their Sr_2RuO_4 sample at 0.93 K.

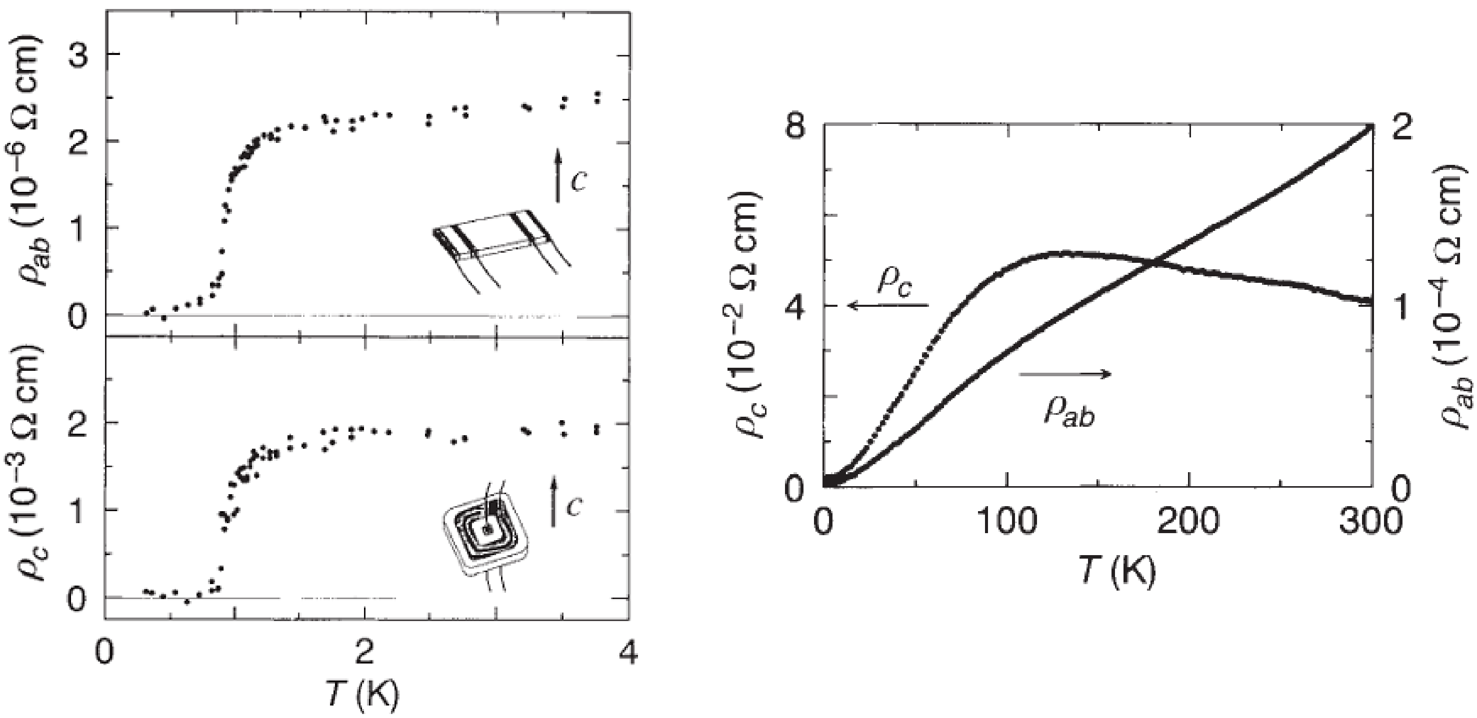

Figure 4.11: left: The low temperature resistivity of Sr_2RuO_4 along a (ρ_{ab}) and c (ρ_c) directions which shows the superconducting transition occurring at 0.93 K, the insets are resistivity electrode attachment arrangements. Right: anisotropy in the resistivity in a and c directions (reprinted from [7]).

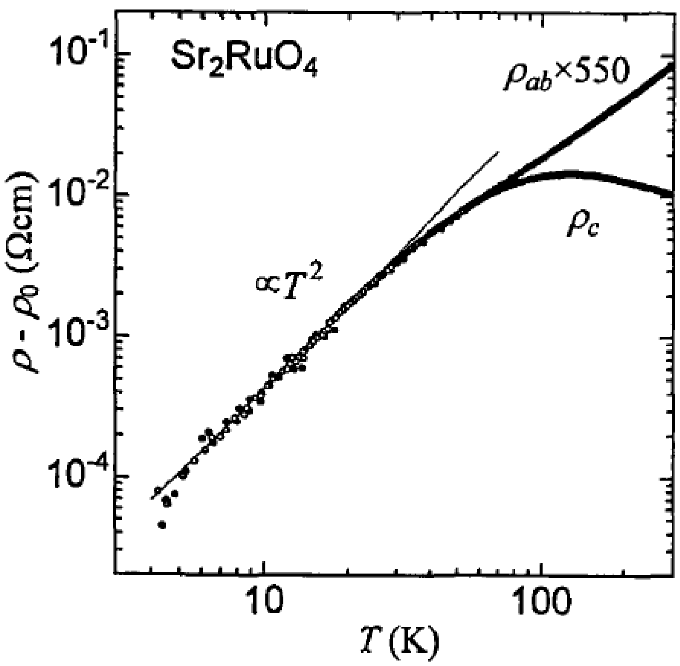

Figure 4.12: The resistivity of Sr_2RuO_4 along a and c directions vs. T on a logarithmic scale. The deviation from Fermi liquid T-squared behaviour happens almost at same temperature for in-plane and out-of plane resistivities (reprinted from [8]).

Maeno *et al.*[8] later studied the Fermi liquid behaviour of Sr_2RuO_4 and they identified T^2 resistivity below 25 K (shown in Figure 4.12). The sample used in these measurements became superconducting at 0.93 K and had a residual resistivity of $\rho_{ab} = 0.9$ $\mu\Omega$cm and $\rho_c = 0.5$ mΩcm. The low temperature resistivity up to about 25 K showed the T-squared Fermi liquid behaviour which indicates that electron-electron scattering is the most significant contribution to the resistivity below 25 K. Above 25 K the resistivity continues to increase but deviates from Fermi liquid behaviour. It can be modeled by $\rho = \rho_0 + BT + A'T^2$ with large T-linear component and much smaller T-squared component [8]. Maeno *et al.* have also modeled both ρ_{ab} and ρ_c with $\rho = \rho_0 + AT^n$ with $n = 1.6$ for temperature range 25-65 K. Above 65 K, ρ_c behaviour diverges from ρ_{ab} and reaches a maximum at 130 K and it shows nonmetallic behaviour above this temperature [8].

4.4 Sr_2RhO_4

Another compound that attracted some attention is Sr_2RhO_4. The crystal structure of Sr_2RhO_4 is tetragonal and various studies such as transport measurements by Shimura *et al.*[34] have shown that it is a metal. Sr_2RhO_4 shows some similar behaviours to Sr_2RuO_4 such as having a high anisotropic resistivity between the ab plane and c directions [9]. In addition, it shows Fermi Liquid behaviour at low T. However, unlike Sr_2RuO_4, Sr_2RhO_4 does not become a superconductor down to 36 mK [9].

A recent study on Sr_2RhO_4 resistivity has been done by Nagai *et al.* [9] Figure 4.13. ρ_{ab} is well described by the Fermi liquid equation $\rho_{ab} = \rho_{ab,0}+A_{ab}T^2$ with $\rho_{ab,0} = 8.6\mu\Omega$cm and $A_{\text{ab}} = 6.26 \times 10^{-3}\mu\Omega$cm K^{-2}. The out-of-plane resistivity $\rho_c(T)$ has a wide peak around 200 K and decreases with increasing temperature above 200 K. ρ_c also shows Fermi liquid behaviour below 24 K and resistivity data is fitted to $\rho_c = \rho_{c,0} + A_cT^2$ with residual resistivity $\rho_{c,0} = 20.1m\Omega$cm and $A_c = 10.55\mu\Omega$cm K^{-2} [9].

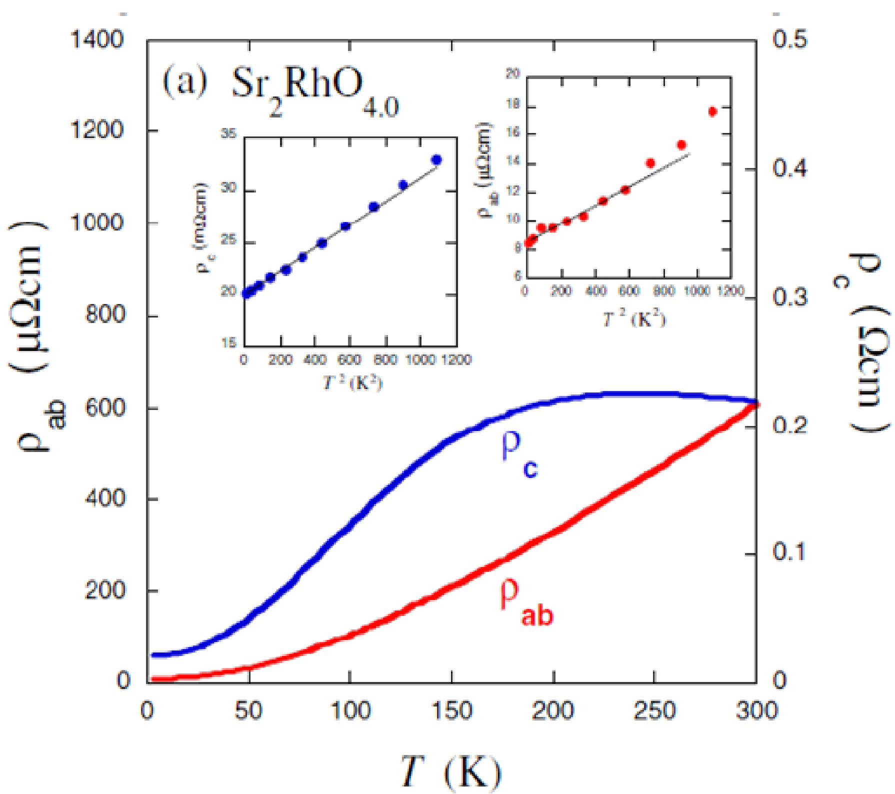

Figure 4.13: The anisotropic in-plane (ρ_{ab}) and out-of plane (ρ_c) resistivities of Sr_2RhO_4 vs. T. The insets demonstrate Fermi liquid behaviour in both the ab plane and the c direction (reprinted with permission from Nagai *et al.*[9]. Copyrighted by the Physical Society of Japan.

Chapter 5

Measurement Techniques

5.1 Four point (Kelvin) method

The simplest tool for measuring resistivity is an ohmmeter connected with two wires to the unknown sample. However, if we need to measure the resistivity of a sample from a significant distance we need to have long wires. The ohmmeter will add the resistance of the wires to its reading to that of the unknown sample and while usually we choose wires with low resistivity, a problem arises when the wires are very long and the resistivity of the sample is very low. As a result the measured resistivity will have a substantial error.

A better way of measuring resistivity is by applying a current I through the sample and measuring the voltage V across it. Then the resistance is calculated from Ohm's law

$$R_{load} = \frac{V}{I} \tag{5.1.1}$$

Since the circuit is a series loop, the current is the same in all the circuit components and if we are only measuring the voltage across the sample, the resistance of the wires is eliminated in our resistance calculation. For the case of distant measurement we will have an accurate result even though we have to use long wires. This method, which eliminates the errors caused by wire resistance, is called the four point or Kelvin method. To measure the resistance using the four point method the sample is cut in the shape of a bar and the wires are connected to four contacts; the contacts at the end of the bar are called the current contacts and are connected to a current supply while the inner

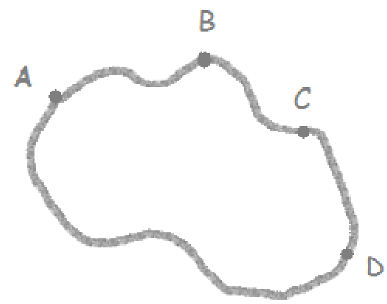

Figure 5.1: Van der Pauw contacts on a sample with arbitrary shape

contacts are the voltage contacts and are connected to a sensitive voltmeter as shown in inset of the left top panel in Figure 4.11. This method is based on an assumption that due to the geometry of the bar, the current stream lines are parallel. We also note that if the material is highly anisotropic the current contacts have to cover the entire end of the sample to assure a uniform current density between the voltage contacts. The four-contact method also eliminates problems associated with the contact resistance between the various components of the circuit such as the material (silver epoxy in our case) used to make the contact between the sample and the wires.

5.2 Van der Pauw method

This method was first introduced by Van der Pauw in 1958 [35] is known as Van der Pauw method. It is a method that can be used to measure the resistivity and the Hall effect of planar samples with arbitrary shapes. Four conditions have to be satisfied for a Van der Pauw measurement:

1- The sample used is flat with uniform thickness.

2-The sample does not have any isolated holes.

3-The contacts are very small compared to the size of the sample.

4-The contacts are at the edge of the sample.

Consider the case where we have a sample satisfying the four conditions above with four contacts A,B,C and D at its circumference as shown in Figure 5.1. We apply the current I_{AB} to the sample which enters though contact A and leaves the sample at contact B. We measure voltage difference $V_C - V_D$

between C and D. We define the resistance $R_{AB,CD}$

$$R_{AB,CD} = \frac{V_{CD}}{I_{AB}} \tag{5.2.1}$$

If we define the resistance $R_{BC,DA} = \frac{V_{DA}}{I_{BC}}$, Van der Pauw showed that the relation

$$e^{\pi R_{AB,CD} d/\rho} + e^{\pi R_{DA,CB} d/\rho} = 1 \tag{5.2.2}$$

is held for resistances $R_{AB,CD}$ and $R_{DA,CB}$ where d is the thickness and ρ is the specific resistivity of the sample. If d is known the equation can be solved for the only unknown ρ.

If the two contacts D and C are located at the line of symmetry and the two contacts A and B are located symmetrically relative to the symmetric line, we have $R_{AB,CD} = R_{DA,CB}$ which gives

$$\rho = \frac{\pi d}{\ln 2} R_{AB,CD} \tag{5.2.3}$$

For general case there is no explicit solution for ρ but we can write ρ as

$$\rho = \frac{\pi d}{\ln 2} \frac{R_{AB,CD} + R_{DA,CB}}{2} f \tag{5.2.4}$$

which f is the numerical function of $\frac{R_{AB,CD}}{R_{DA,BC}}$ defined by

$$\exp\left(-\frac{\ln 2}{f(x)}\right) \cosh\left(-\frac{x-1}{x+1}.\frac{ln2}{f(x)}\right) = \frac{1}{2} \tag{5.2.5}$$

with $x = \frac{R_{AB,CD}}{R_{DA,BC}}$ [35]

5.3 Home-built immersion probe

For resistivity measurements at different temperatures, we constructed a simple immersion probe. Figure 5.2 is the schematic picture of an immersion

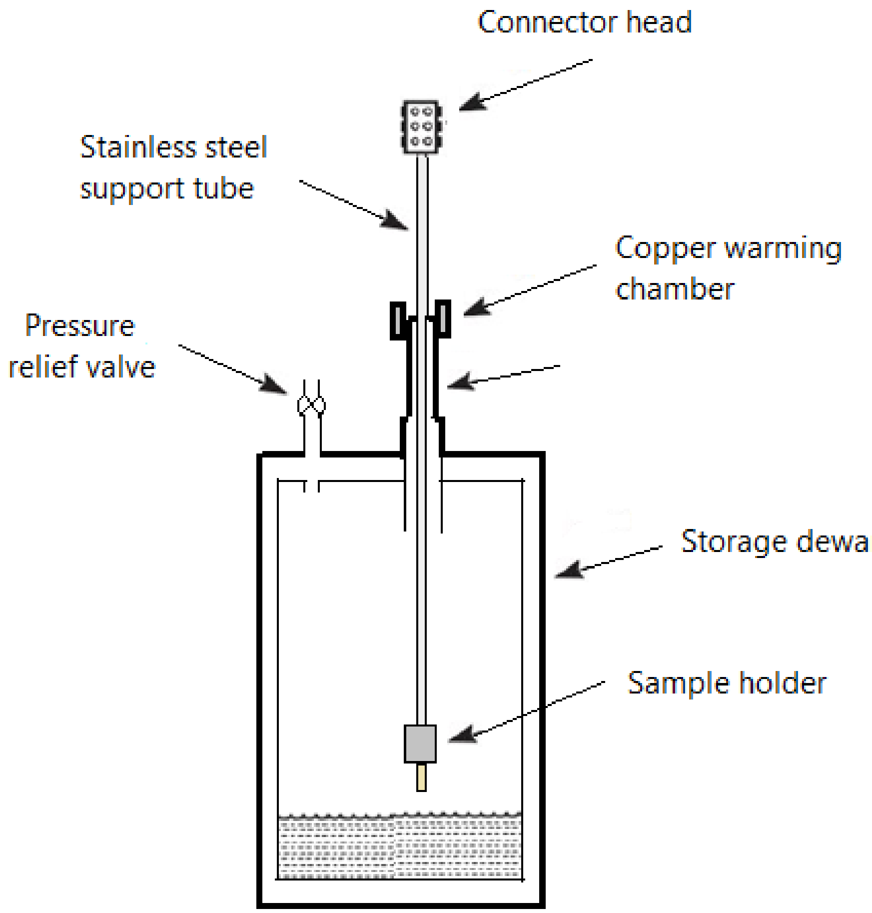

Figure 5.2: Schematic picture of an immersion probe

probe. For low temperature measurement the end of the probe can be immersed in liquid helium and for higher temperatures the temperature can be changed by raising the sample above the liquid helium surface. Since the temperature gradient of helium gas above the liquid surface is not constant it is not an easy task to change the temperature at a constant rate. So the easiest way to sweep the temperature is drifting the temperature and collecting data at crude temperature steps [36].

The construction of the different part of the immersion probe is described in the following. The sample holder should be made of a material with sufficient thermal mass in order to have stable temperature. Furthermore, it needs to be a material with a high thermal conductivity to make sure that the sample and the thermometer are at the same temperature [36].

Figure 5.3: The sample holder built at McMaster University

For this purpose, aluminum is used which has fairly high thermal conductivity, about $205\frac{\mathrm{W}}{\mathrm{m.K}}$. To allow measurements above 4.2 K a stick made of brass is attached to the end of sample holder to be immersed in the liquid. A temperature gradient can then be established between the helium surface and the sample with a heater attached to the sample holder. As Figure 5.3 shows another plate of aluminum is used to mechanically protect the sample and wires while the probe is being moved. The metal cryogenic dewar is already shielded so we do not need to shield the sample holder from thermal and electromagnetic radiation. The sample is mounted on a piece of sapphire which is held by aluminum clips.

For temperature measurements a Cernox thermometer is used which is attached on the the sapphire plate close to the sample using a brass clip. Cernox (Zirconium-oxynitride) is a semiconductor thermometer which is one of the best thermometers for temperature range from 0.3 K to room temperature since it has an accuracy of 5 mK at 4.2 K and better than 1% above 10K. It also has good thermal reproducibility and long term drift which makes it a very good sensor for the entire temperature range from liquid helium to room temperature [36].

A 100 Ω resistor is used as a heater which is connected to a power supply to have better control over the temperature and the change in the drift rate (Figure 5.3). All the wires are heat sunk by winding them around the screws on the sample holder to make sure that the sample holder, the sample and the thermometer are at the same temperature.

For the supporting parts such as the probe tube we need a material that is not brittle and has low thermal conductivity in the cryogenic temperature range. Stainless steel is one of the best candidates for the supporting tube since

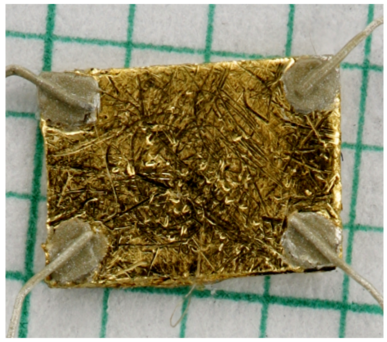

Figure 5.4: Van der Pauw contacts on a gold sample prepared in our lab at McMaster University

it has a fairly low thermal conductivity from low to high temperature and it is mechanically strong. Furthermore it is inexpensive and easily available in the form of tubing. It is important to use the material with fairly matched thermal expansion coefficient for different parts such as sample holder and supporting tube which are joined. The large difference between thermal contractions can cause ripping the pieces apart. The metals used for sample holder (aluminum), supporting tubes (stainless steel) and the joint between which is made of brass have similar expansion coefficients.

5.4 Sample preparation

For the first few measurements (for $URu_{2-x}Re_xSi_2$ with three doping levels) silver epoxy and silver paste were used for the electrical contacts to the samples. A small amount of silver epoxy was first placed at the corners of the sample for Van der Pauw geometry. Then the sample was heated in a furnace for an hour at 400 C. Then the silver wires were attached on top of the epoxy contacts by using silver paint. Silver paint is cured at room temperature for about half an hour. However, the contacts made this way are weak mechanically (Figure 5.4).

Later we used Dupont 6838 epoxy to attach the electrodes to the samples. Dupont 6838 epoxy is cured at 400 C for 5 minutes and it becomes very strong, making it easier to wire the sample. In addition, after wiring the sample, we place it on a small sapphire plate and attach the wires to the plate (as shown in Figure 5.5) so the wires do not come off or break while we solder the wires

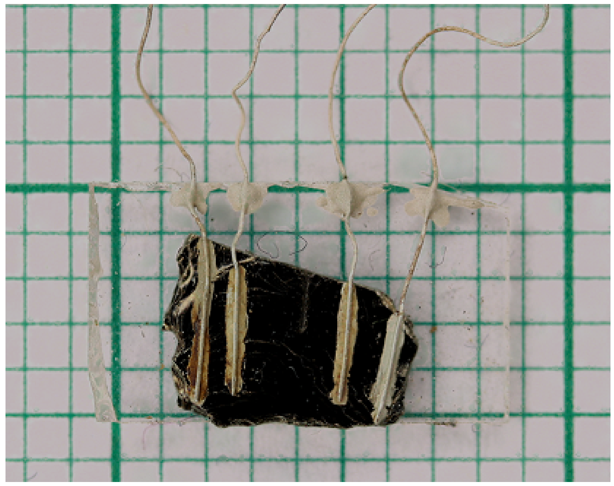

Figure 5.5: Four point AC contacts on $URu_{2-x}Fe_xSi_2$ with $x = 0.2$ sample on a sapphire plate prepared in our lab at McMaster University

to a connector or mount it on the sample holder.

5.5 Testing the immersion probe

We used the voltmeter and the current source which are parts of the Oxford Cryostation Maglab system at McMaster University. Since we were not using the Oxford sample holder and cryostat system, we could not control the temperature using the Oxford thermometer and heater sensor. Instead we used a current source to heat up the resistor and mechanically moving the sample holder to control the temperature. We run LabView software for resistivity versus time.

Each resistivity point measurement with this system took 60 seconds and we set the delay time (which is the time between every temperature point) to 80 second to have enough time to manually change the temperature and let it stabilize. Therefore, sweeping the temperature from liquid helium temperature to room temperature in 1 K steps took about about ten hours.

The sample that was used for the first test run was URu_2Si_2 with Re doping, $x = 0.07$, which was wired using the silver paint method. As we can see in Figure 5.6 starting from room temperature as the temperature is lowered the resistivity first goes up until it reaches its maximum around 78 K and then drops rapidly. We observe a small kink at the HO transition at 15.7 K. The derivative of the resistance shows that the noise level is very high for this test

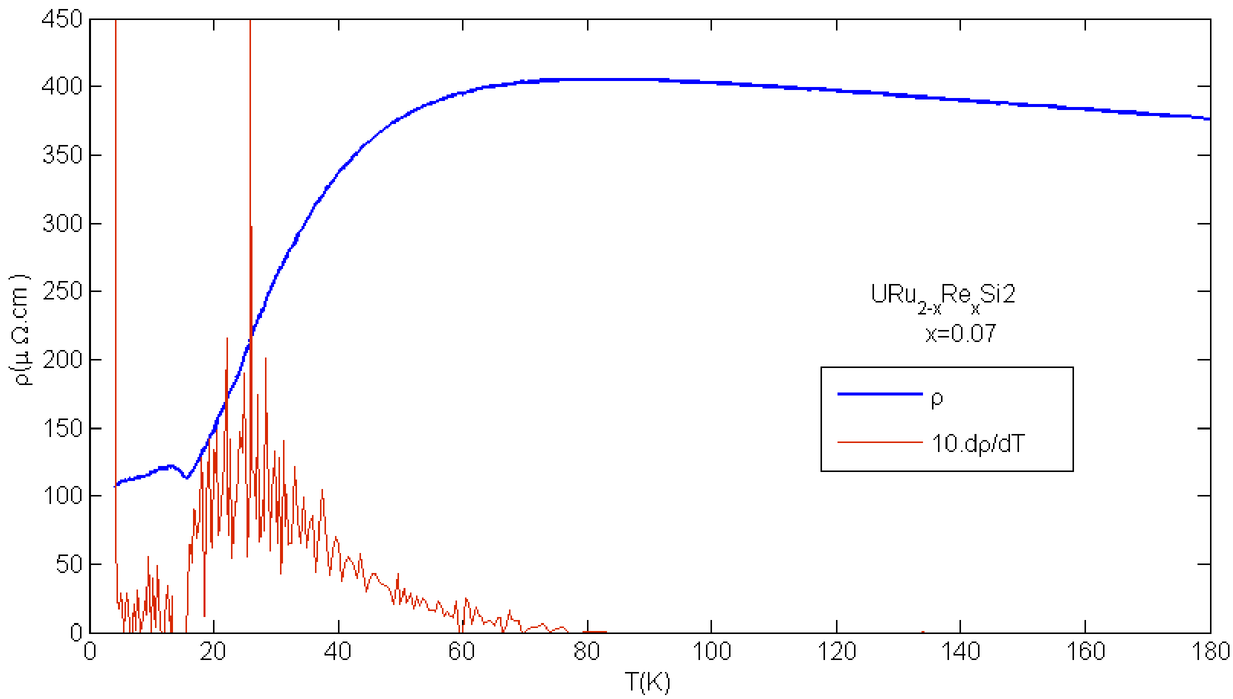

Figure 5.6: Van der Pauw dc resistivity of $URu_{2-x}Re_xSi_2$ with $x = 0.07$ with HO temperature T_0 measured with the immersion probe.

run.

There are severeal sources of noise. The main source of noise is probably an uncertainty in temperature. The controller is set manually by setting the current for the heater and moving the probe. These are not reliable ways of stabilizing temperature. Another source of noise can be improper probe wire shielding or current source fluctuations.

5.6 The Oxford cryostat

One of the main issues with the measurements of low resistivity samples is the presence of noise. As we observed in previous sections, the noise level in dc resistivity measurements can be fairly high. It was found that noise can come from different sources, such as the voltmeter or the current source and also from external sources such as pick-up from other electrical equipment around the measurement set up. A common way to reduce the noise level is to

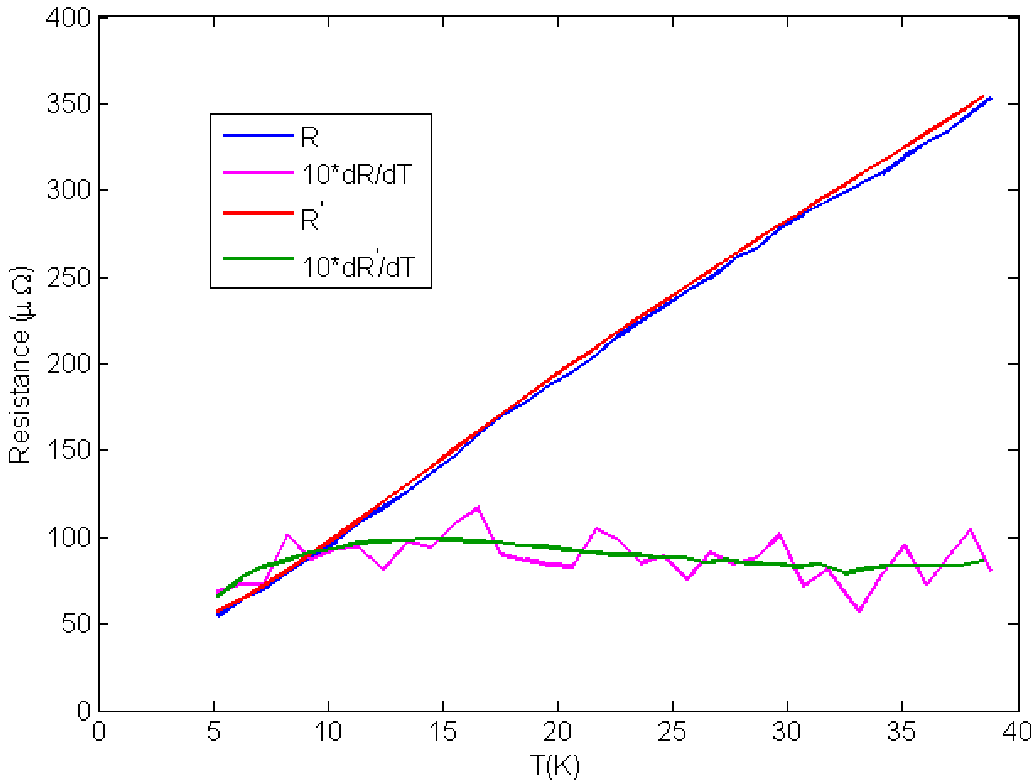

Figure 5.7: The effect of optimization of parameters on noise. The blue line represents the resistance of Sr_2RuO_4 using an AC current of 10 mA, 20 Hz frequency, time constant = 5 sec and a delay time = 5 sec (the pink line is $10dR/dT$). The red line is resistance (its first derivative (green line)) measured using an AC current of 60 mA with 30 Hz frequency, time constant = 30 sec and delay time = 60 sec. A major improvement in the signal to noise ratio can be obtained by increasing the observation time and the current.

use an AC lock-in amplifier. A lock-in amplifier uses the technique of phase sensitive detection which singles out an AC signal at a precise test frequency and rejects all other frequencies. Furthermore, thermoelectric effects which cause inaccuracy in dc resistance measurement is reduced by using this technique.

5.7 Four point AC resistance measurement

The Oxford AC current probe was used for Sr_2RuO_4. This instrument is not programmed for the Van der Paw method and can only be used for four point resistance measurements.

For AC resistance measurement we need to set the frequency of the alternating current, the lock-in time constant, the lock-in frequency and delay time that allows for the temperature to stabilize.

Figure 5.7 shows the resistance for two sets of measurements. For the first measurement (blue line) the is current 10 mA, the frequency 20Hz and time constant 5 seconds. We increased the current to 60 mA, the frequency to 30 Hz, the time constant to 30 seconds and delay time to 60 seconds for the second set, shown as a red line. We can see that we have much less noise in the derivative of second set of measurements (the green line) than the first set (the pink line). This is mostly due to the fact that for the first run the voltage is scanned and averaged over 100 ac cycles while in the second run is averaged over 900 cycles. Furthermore, by waiting longer between two data points, the time for stabilizing temperature is longer so we have less noise due to temperature variations.

5.7.1 Temperature drifting

As we saw in the previous section by using AC current with a large time constant and delay time for four point AC resistance measurement, we can reduce the level of the noise. However, if we run the measurement over a wide range of temperature it will take a long time to sweep the temperature (more than 12 hours) to take enough data points. Another way of sweeping the temperature is by drifting it, which is much faster. The temperature drifting method is available in the Oxford cryostat AC four-point measurement program. They use the same set of parameters that we used for AC resistance except that by setting the drift rate we can control how fast we want to sweep the temperature and how many data points we would like to take. The problem that arises with temperature drifting is that we do not wait for the temperature to be stabilized before taking the data at each temperature. In order to have accurate data we set the drifting rate to a very low value and we take more data point at each temperature. Furthermore, by running the measurement from low to hight T followed by high to low T and and then taking the average over the two data sets, we can have more accurate data that cancels out the temperature delay between the sample and the thermometer. This is based on the fact since the temperature is not stabilized, starting form low to hight the

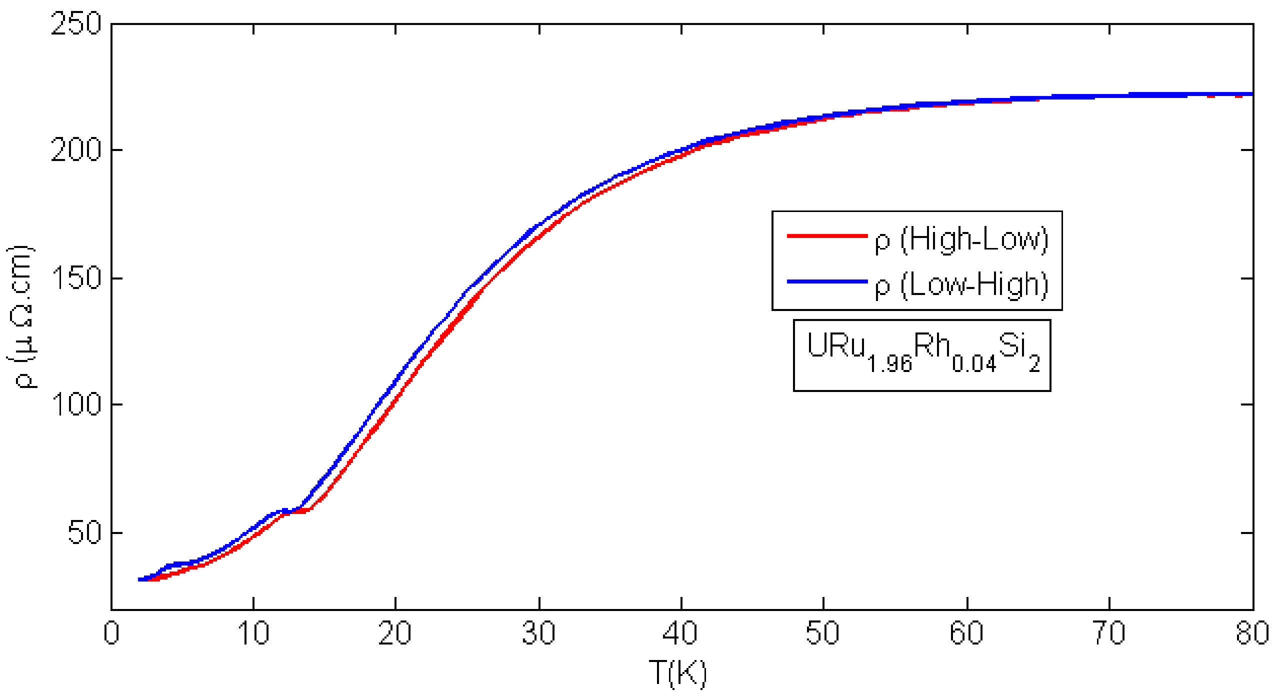

Figure 5.8: The resistivity of $URu_{2-x}Rh_xSi_2$ with $x = 0.04$ vs. T using AC four point drifting method, the drift rate is 1 K/min, the red line is drifting from high to low temperature and the blue line is from low to hight temperature. The temperature difference between the two measured data sets at the same resistivity is about 1.4 K

temperature measured by the thermometer is behind the temperature of the sample while by sweeping the temperature from high to low T the temperature measured by the thermometer is ahead of the actual temperature so the actual temperature is somewhere between the temperature measured in each case. An example is shown in Figure 5.8. The average of the up and down drifts is a good estimate of the actual temperature. The average difference in temperature of the two sets was about 1.4 K so we estimate the error in temperature is less than half of that figure.

After testing different drift rates, we set the drifting rate to 1 K/min, the time constant to 1 sec, the frequency to 50 Hz, the delay time 1 second and took the average over 5 data points for all the AC resistance measurements in chapter 6. Since it takes 5 seconds to collect each data point, it takes 1.5 hours to sweep the temperature from 2–200 K. Therefore, the total AC resistance measurement (low to high T and high to low T) takes 3 hours which is much shorter than the van der Pauw method.

Chapter 6

Results

6.1 Introduction

In this chapter we present the experimental results of the dc resistivity and its derivative for URu_2Si_2 doped with rhenium, iron and rhodium, as well as Sr_2RuO_4. We analyze the data in terms of Fermi liquid theory that predicts a T^2 variation of the resistivity with temperature and a linear in T variation of the derivative (with a zero intercept).

6.2 $URu_{2-x}Re_xSi_2$

The measurement of the resistivity of the parent compound URu_2Si_2 is not part of this thesis. To compare these data with our doped samples we use the high resolution, low noise, data of Matsuda *et al.* [3] who kindly supplied us with their data. The $URu_{2-x}Re_xSi_2$ samples with $0.02 \leq x \leq 0.1$ were grown by Dr. Maple's group. The resistivity measurements on Re doped samples were done at McMaster University with the Oxford cryostat. We performed van der Pauw resistivity measurement with a DC current of 60 mA.

6.2.1 Resistivity and its first derivative

Figure 6.1 displays the in plane resistivity (ρ_{ab}) for different Re doping values from 4 K to 90 K. The resistivities have the same general profile as the ones measured in previous studies [4]. Figure 6.2 (a) shows the resistivity of $URu_{2-x}Re_xSi_2$ for different Re doping values near the HO order transition. As

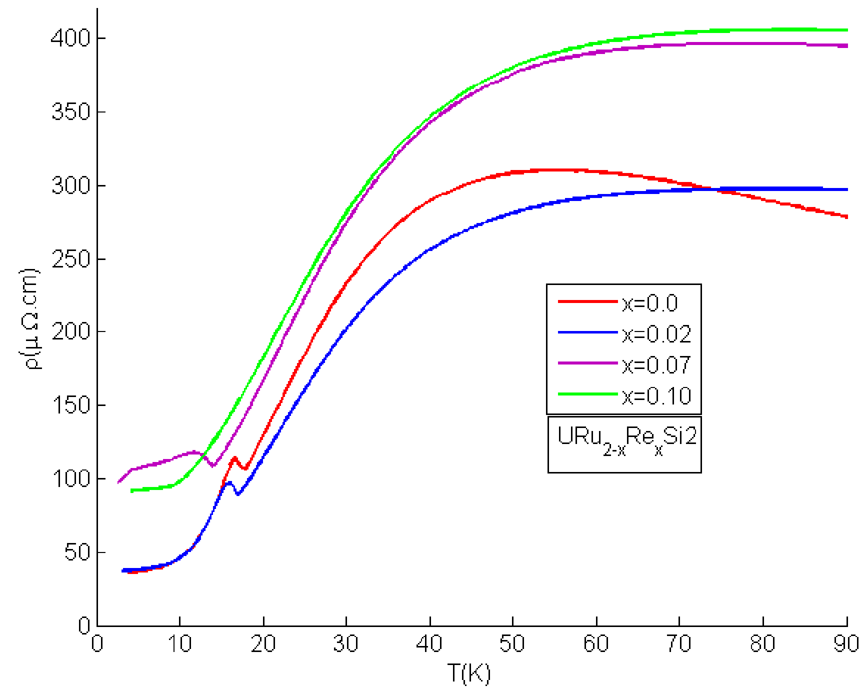

Figure 6.1: The resistivity of $URu_{2-x}Re_xSi_2$ with different x values

can be seen, T_{HO} appears as a kink in the resistivity, at 17 K in the unroped material decreasing in temperature as x increases up to 0.07. For $x = 0.1$ the hidden order transition is broadened and no longer shows a peak. The resistivity measured by Dr Maple's group shows a slight rise at 10 K as evidence of the HO transition for $x = 0.1$, but they could not see it for $x = 0.12$ [4]. It is possible that our sample $URu_{2-x}Re_xSi_2$ with 0.1 might have slightly higher Re doping than 0.1.

Figure 6.2 (b) shows the first derivative of the resistivity with respect to T and as we can see, the negative region of the derivative broadens with doping x up to 0.07 but for $x = 0.1$ the transition anomaly does not go negative but it is still visible as a minimum in the derivative. We can make a rough estimate of the transition temperature at $x = 0.1$ as 8 ± 2 K.

6.2.2 Fermi liquid fit

The parent compound URu_2Si_2 shows Fermi liquid behaviour at temperatures above the HO transition up to 25 K as shown by Nagel *et al.* [2] in a high

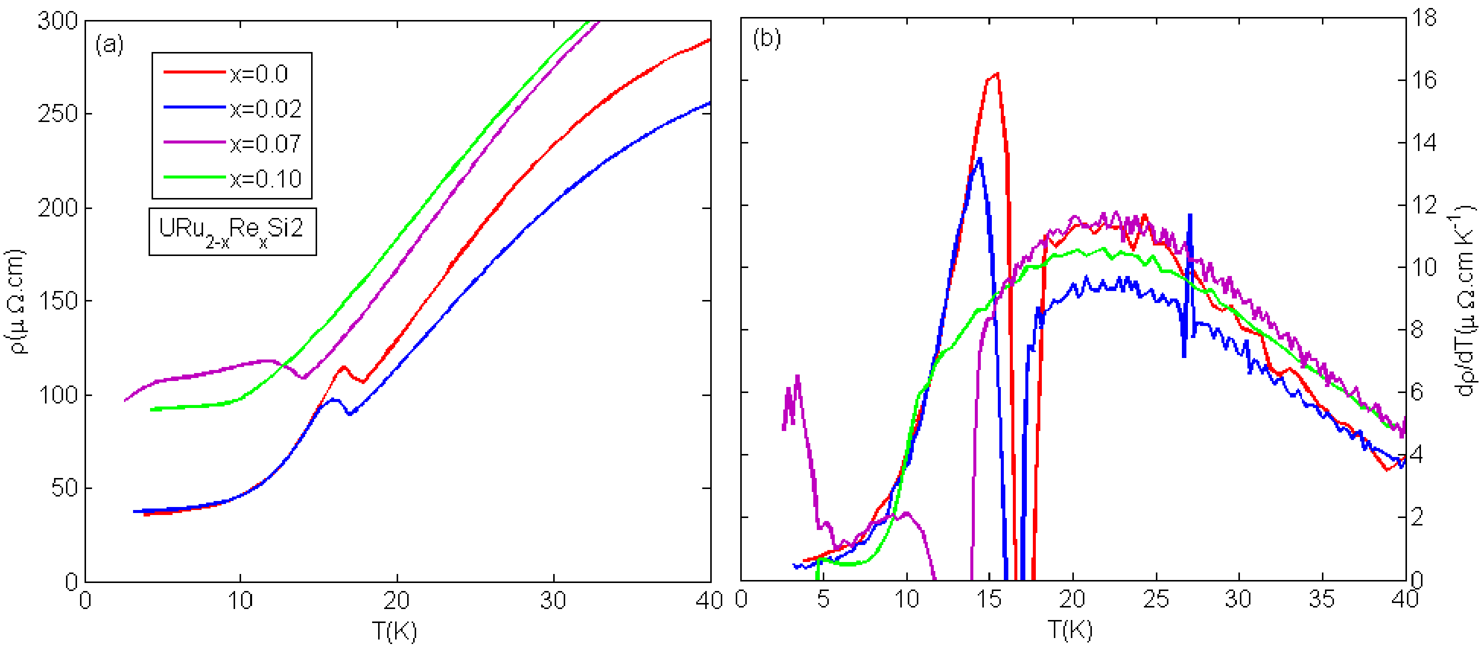

Figure 6.2: (a) The resistivity for $URu_{2-x}Re_xSi_2$ vs. T near the HO transition for different values of x. The T_{HO} is shifted to lower temperature with increasing concentration of Re doping for $0.02 \leq x \leq 0.10$. The HO transition broadens for $x = 0.10$. (b) the derivative of the resistivity $d\rho/dT$ for $0.0 \leq x \leq 0.10$

Table 6.1: The fit parameters of $URu_{2-x}Re_xSi_2$ with different values of x in the Fermi liquid region using the formula $d\rho/dT = 2AT + B$

x	A($\mu\Omega$.cmK^{-1})	$B(\mu\Omega.cmK^{-1})$
0.0	0.2655	0.06
0.02	0.2321 ± 0.1343	0.0
0.07	0.2929 ± 0.23044	0.0
0.10	0.2966 ± 0.0746	0.0

resolution study of the *frequency dependence* of the optical resistivity. The dc resistivity on the other hand, shows that the Fermi liquid region is very narrow above the HO transition. For a consistent analysis we decided to adopt the following, somewhat arbitrary, criterion to choose the temperature range where we fit our data: from $T_{\mathrm{HO}}+1$ K to $T_{\mathrm{HO}}+3$ K for all Re dopings, in other words, a 2 Kelvin range starting one degree above the transition. We justify the starting temperature by noting that there is a narrow region, roughly 1 K above the transition (here defined where the derivative $d\rho/dT$ goes to zero), presumably associated with critical fluctuations and where $d\rho/dT$ changes rapidly with temperature. We fitted $d\rho/dT$ to the function $d\rho/dT = 2AT + B$ using the MATLAB curve fitting tool (cftool) Figure 6.3 (a-d). The fit parameters A and B are summarized in table 6.1

6.2.3 Gapped Fermi liquid fit

For fits of the resistivity vs. T in the HO state we used the fitting formula 4.2.1, shown for different Re concentrations in Figure 6.4. We have done the fitting analysis using the MATLAB curve fitting tool cftool. The fitting parameters are gathered in table 6.2. As expected from chapter 4, The HO gap decreases by increasing the amount of Re doping. There is a notable increase in the residual resistivity with doping. Also notable is the decrease in the inelastic scattering in the HO state: the scattering is presumably dominated by the elastic scattering from the Re atoms.

6.3 $URu_{2-x}Fe_xSi_2$

The sample of $URu_{2-x}Fe_xSi_2$ with $x = 0.1$ was grown by the Maple group. The other two Fe doped samples with $x = 0.2$ and 0.3 were grown by Murray

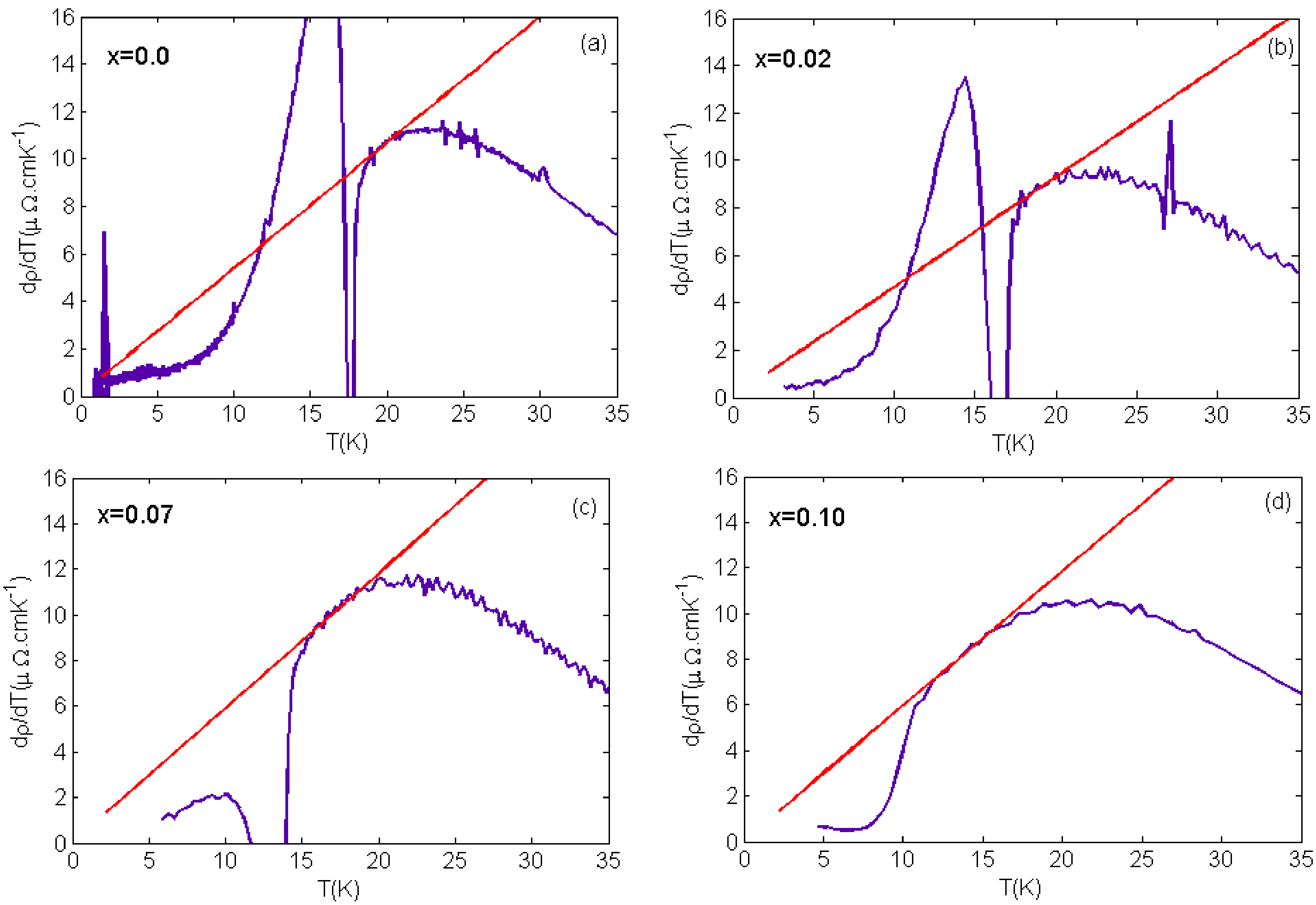

Figure 6.3: (a)-(d) The blue curves are the derivatives of ρ with respect to T for $URu_{2-x}Re_xSi_2$ with different values of x. The red lines represent the Fermi liquid fit $d\rho/dT = 2AT + B$ for temperature ranges of (a) 18.5–20.5 K, (b) 18–20 K, (c) 15–17 K and (d) 12–16 K

Table 6.2: The fit parameters of $URu_{2-x}Re_xSi_2$ with different values of x in the HO state using the formula 4.2.1

x	$\rho_0(\mu\Omega$.cm)	B($\mu\Omega$.cmK^{-2})	A($\mu\Omega$.cmK^{-2})	$\Delta(K)$	T_{HO}
0.0	1.29	4589	1.22	78	17.81
0.02	36.81	3000	0.05	68.68	17
0.07	105	30	0.09	40.77	13.89

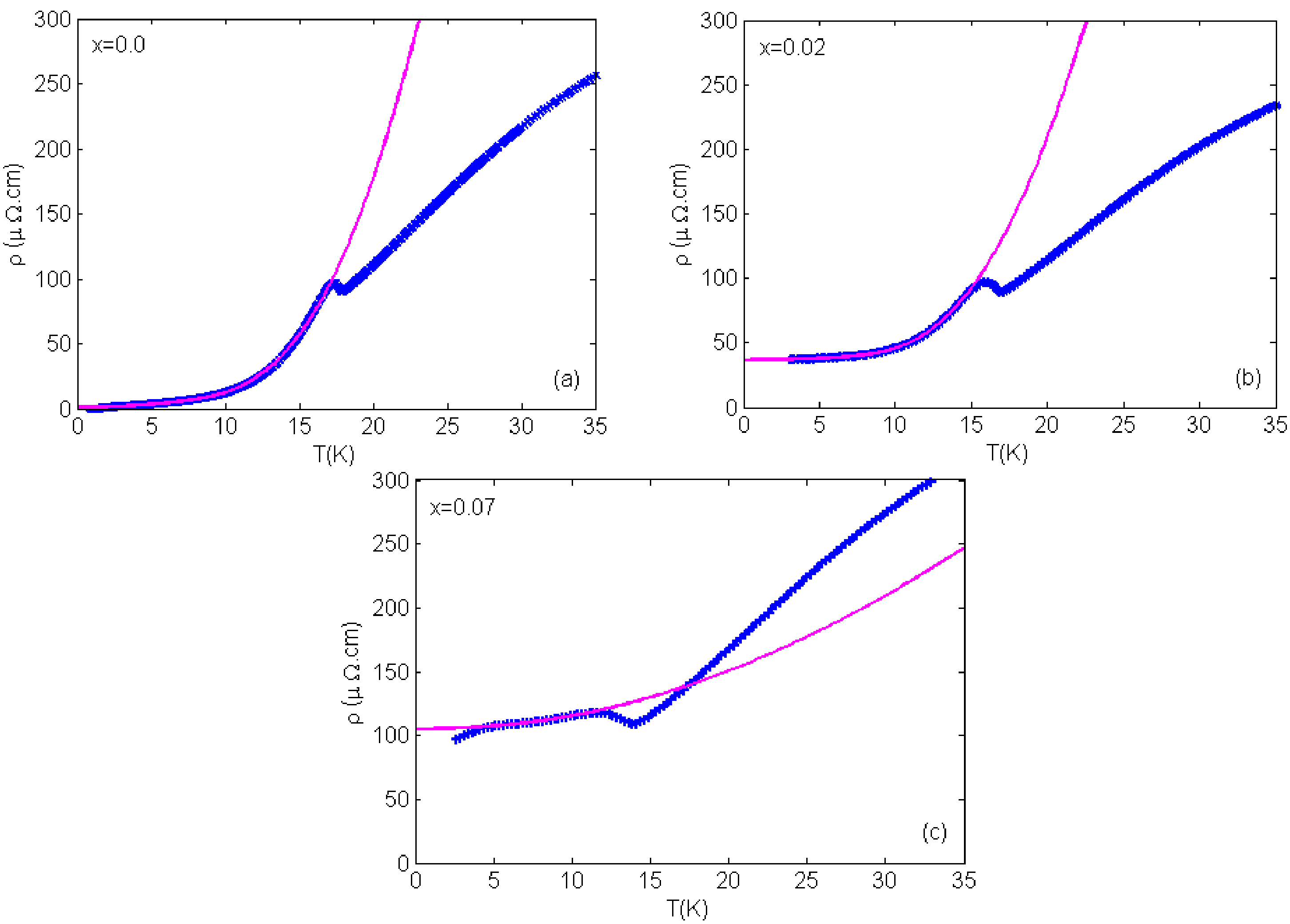

Figure 6.4: (a)-(c) The blue curves show ρ vs. T for $URu_{2-x}Re_xSi_2$ with different values of x. The pink curves represent the fit in the HO state using formula 4.2.1

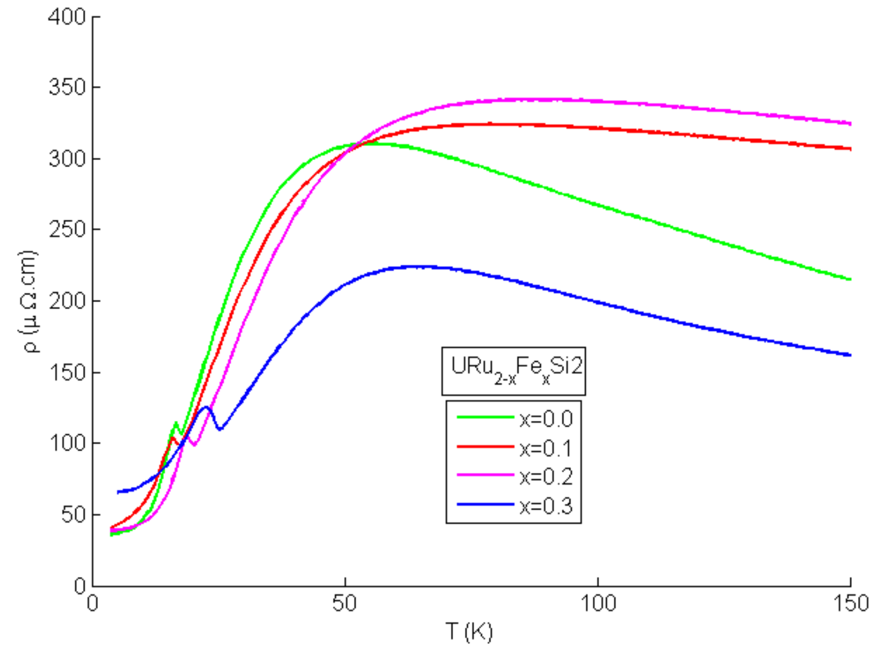

Figure 6.5: The resistivity of $URu_{2-x}Fe_xSi_2$ vs T for different Fe doping values

Wilson, Ph. D. candidate of Dr. Graeme Luke's group at McMaster University. The $\rho(T)$ measurements were carried out in the Oxford Maglab cryostat using the four point AC resistance with the T drift method. In order to get accurate temperature data we performed resistance measurements by moving from low to high T's and vice versa and took the average of the two data sets.

6.3.1 Resistivity and its first derivative

Figure 6.5 (a) shows the in plane resistivity ρ_{ab} for a number of Fe concentrations x as a function of temperature. The resistivity for the three values of x in the HO state is illustrated in Figure 6.6. T_{HO} is detectable as a small peak or an anomaly in $d\rho/dT$. It can be seen that T_{HO} increases with x and the kink associated with it in $\rho(T)$ broadens. The broadening is also visible in $d\rho/dT$ inflection at HO phase transition, Figure 6.6 (b).

6.3.2 Fermi liquid Fit

As expected, we can see the Fermi Liquid behaviour T-squared for various x values Figure 6.7 (a)-(c). $d\rho/dT$ data have been fitted to the Fermi liquid equa-

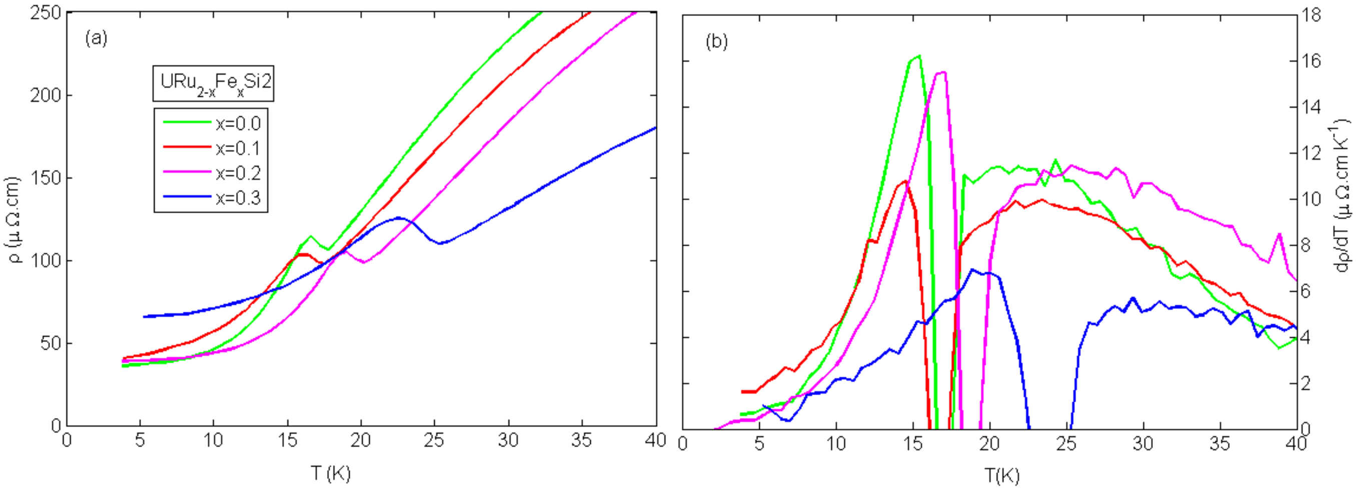

Figure 6.6: (a) The resistivity of $URu_{2-x}Fe_xSi_2$ vs. T around the HO/LMAFM transition. $T_{\mathrm{HO/LMAFM}}$ is shifted to higher temperature with increasing x, (b) the derivative of ρ with respect to T for different x values

Table 6.3: Fit parameters of $URu_{2-x}Fe_xSi_2$ with different values of x using the formula $d\rho/dT = 2AT + B$

x	$A(\mu\Omega.cmK^{-2})$	$B(\mu\Omega.\mathrm{cm}K^{-1})$
0.1	0.21 ± 0.51	0.42 ± 19.82
0.2	0.18 ± 0.41	0.0
0.3	0.089 ± 0.008	0.0

tion $d\rho/dT = 2AT + B$ in the temperature range $T_{\mathrm{HO}}+1 \leq T \leq T_{\mathrm{HO/LMAFM}}+3$ using MATLAB. The fit parameters are shown in table 6.3

6.3.3 Gapped Fermi liquid Fit

The resulting fits of low temperature $\rho(T)$ using gapped Fermi liquid formula are presented in Figure 6.8 (a)-(c). The gap and residual resistivity values for different x obtained via fits to equation 4.2.1 are summarized in table 6.4. The HO transition gap has its maximum value at $x = 0.2$ which is in agreement with previous studies of Fe doping effects on HO/LMAFM phase

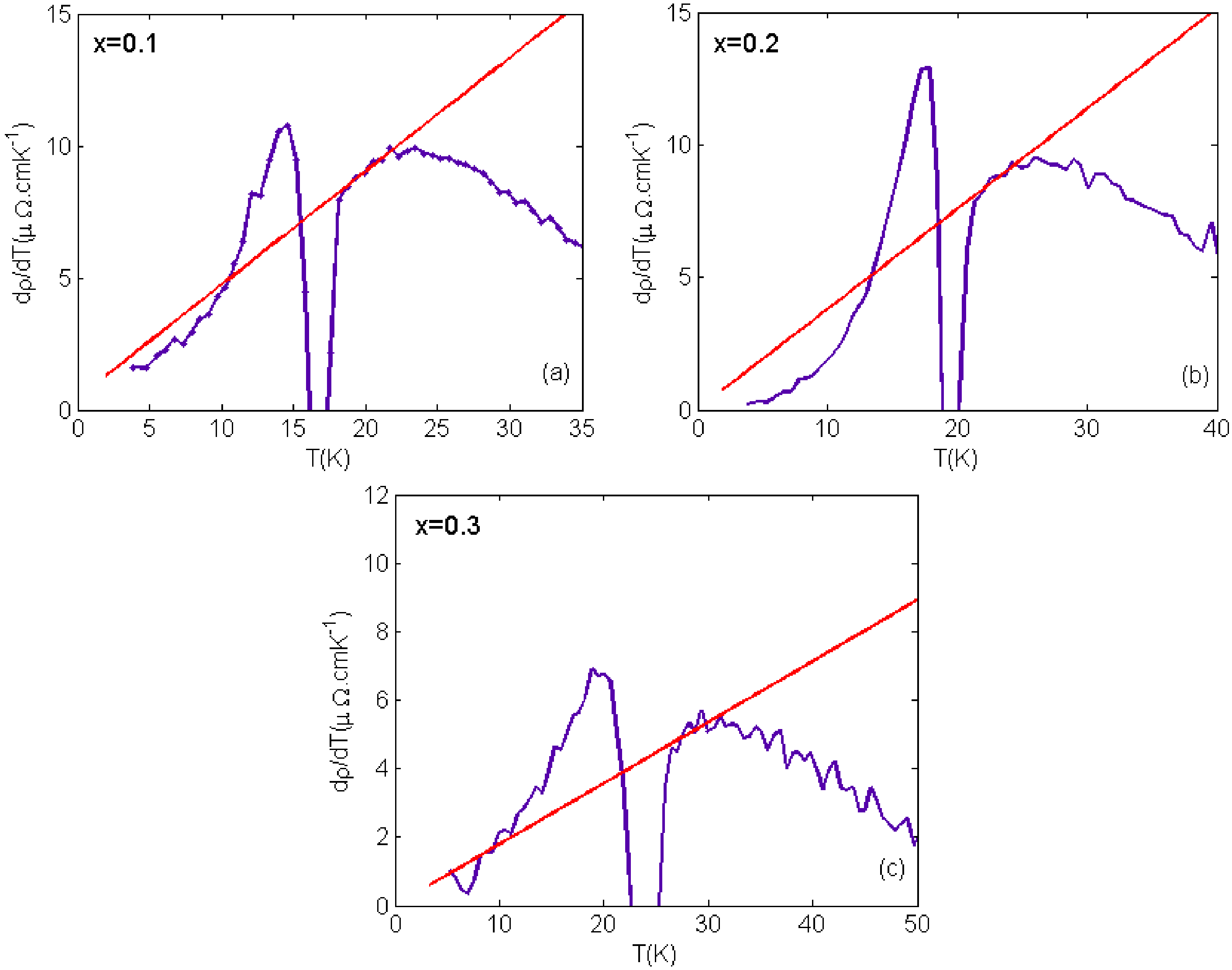

Figure 6.7: The curves a-c show the temperature derivative of the resistivity for $URu_{2-x}Fe_xSi_2$. The pink straight lines are the fit lines $d\rho/dT = 2AT + B$ for the temperature ranges: (a) 18.5-20.5 K with $T_0 = 17.55K$, (b) 21.2-23.2 K with $T_0 = 20.18K$ and (c) 26.3-28.3 K with $T_0 = 25.27K$

Table 6.4: The fit parameters of $URu_{2-x}Fe_xSi_2$ with different values of x in the gapped Fermi liquid region using the formula 4.2.1

x	$\rho_0(\mu\Omega.cm)$	$B(\mu\Omega.cmK^{-2})$	$A(\mu\Omega.cmK^{-2})$	$\Delta(K)$	$T_{\mathrm{HO}}(K)$
0.1	37.88 ± 7.15	3165 ± 10563	0.175 ± 0.107	80 ± 57.35	17.55
0.2	36.47 ± 0.69	4654 ± 2848	0.066 ± 0.009	92 ± 10.1	20.18
0.3	61.29 ± 0.86	783 ± 342	0.09 ± 0.86	85 ± 11.02	25.27

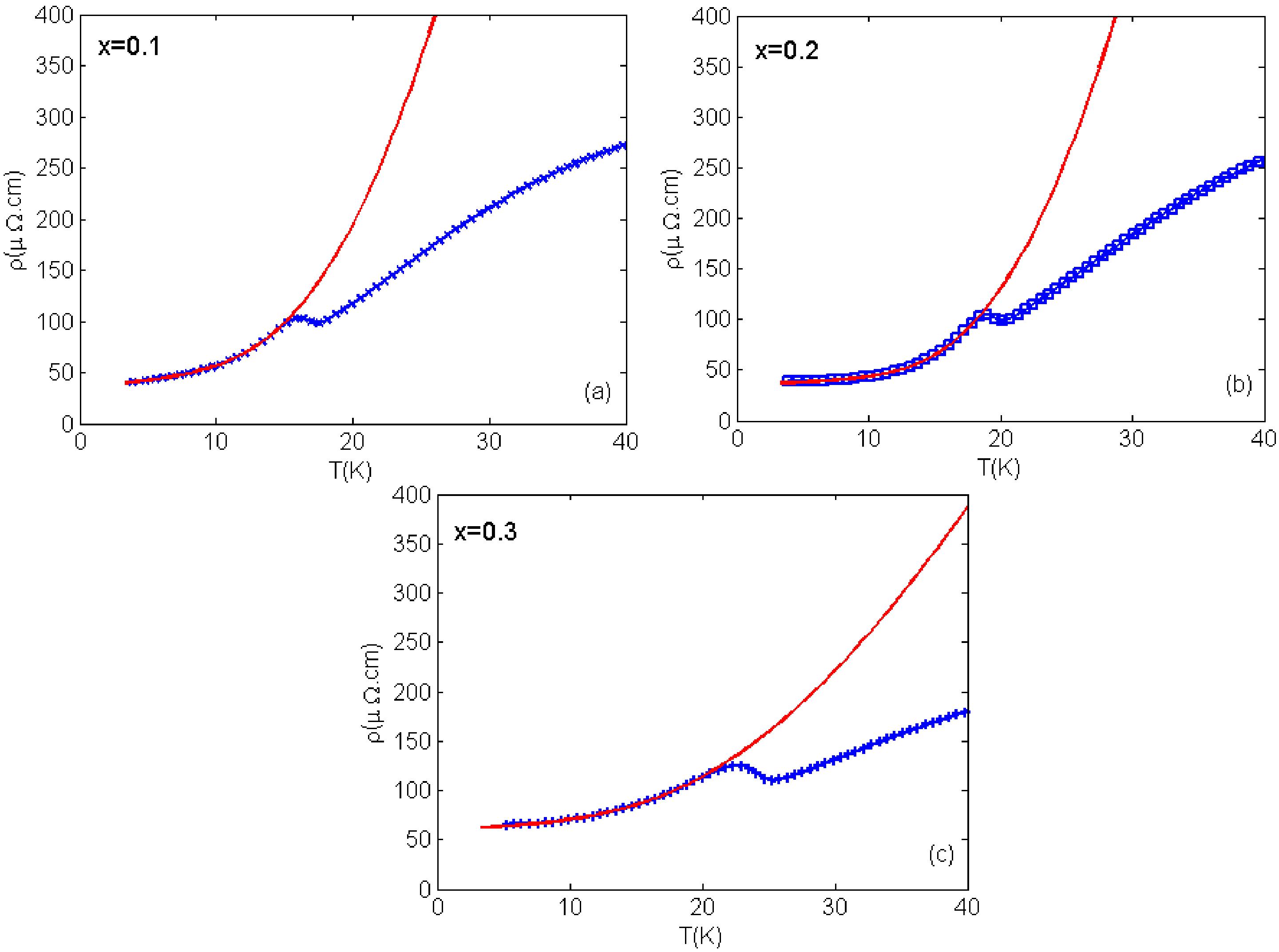

Figure 6.8: Plots a-c show the resistivity ρ vs. T for $URu_{2-x}Fe_xSi_2$ with different doping values of x, the red curves are the fit in the gapped Fermi liquid region using formula 4.2.1

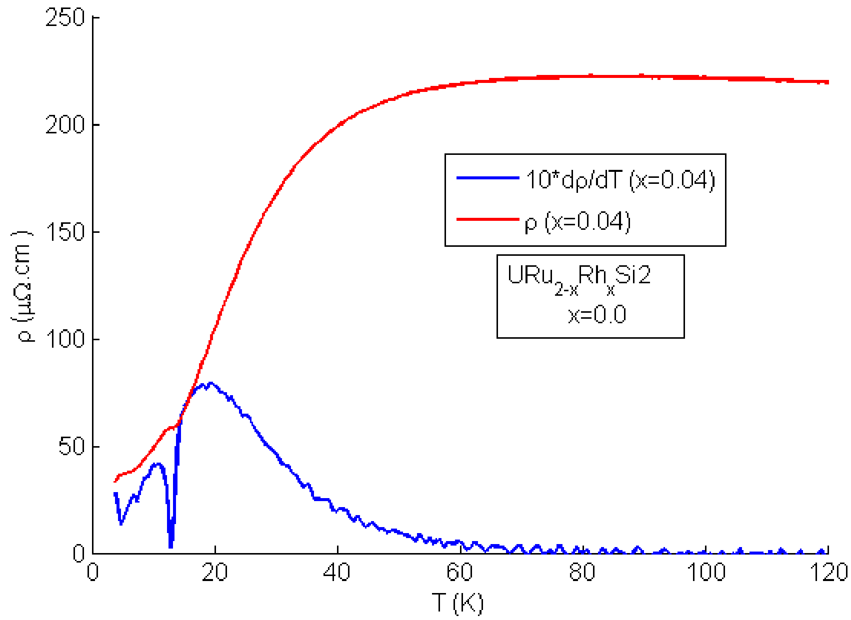

Figure 6.9: The resistivity ρ (red curve) of $URu_{2-x}Rh_xSi_2$ with x = 0.04 and the derivative of ρ with respect to T (blue curve)

6.4 $URu_{2-x}Rh_xSi_2$

$URu_{2-x}Rh_xSi_2$ with $x = 0.04$ was the only available rhodium doped sample for resistivity measurements. The sample was grown by Dr Travis Williams, a former PhD candidate of Dr Graeme Luke at McMaster University. We have measured resistivity by means of AC resistance temperature drifting technique.

6.4.1 Resistivity and its first derivative

As it is shown in Figure 6.10 (a), by adding a small amount of Rh, $x = 0.04$, the HO peak flattens and $T_{\rm HO}$ decreases from 17.8 to 13.35. This change is also visible in $d\rho/dT$ as the minimum detected at the HO transition for $x = 0.04$ widens.

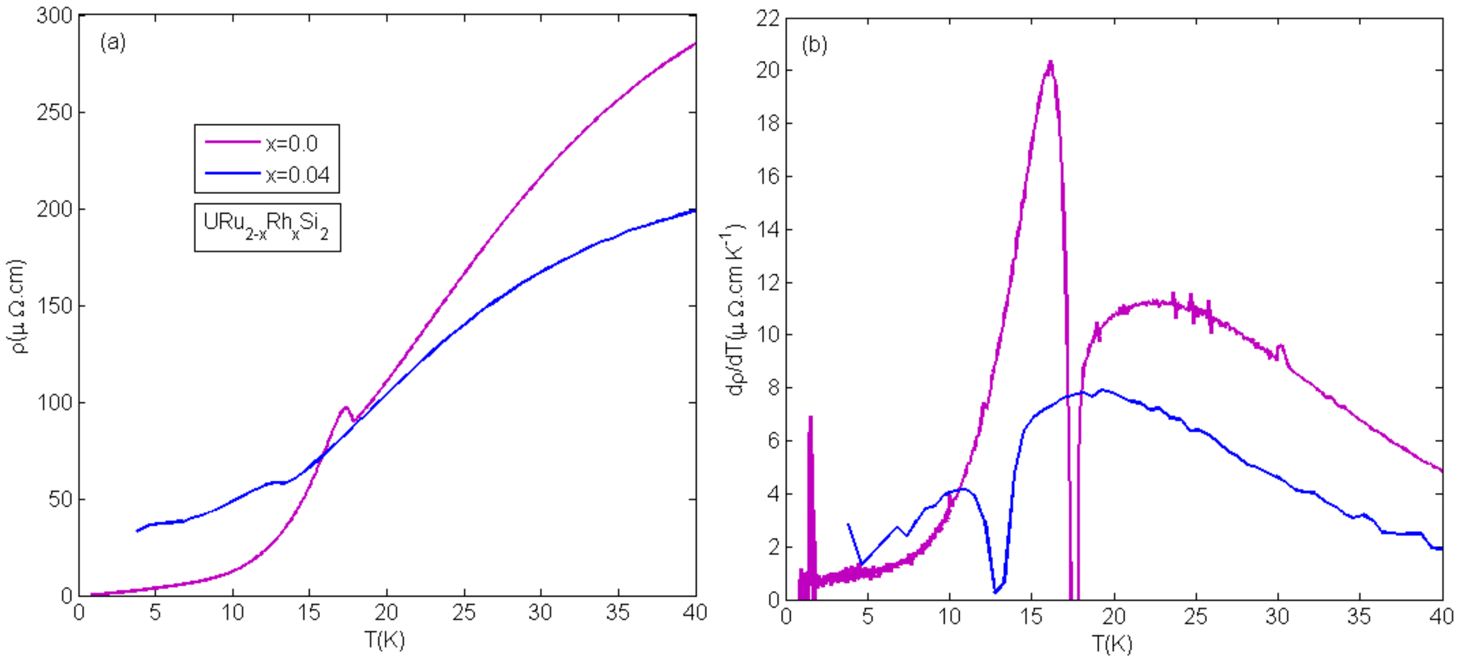

Figure 6.10: (a)The resistivity ρ of $URu_{2-x}Rh_xSi_2$ as a function of T is getting suppressed and shifted to lower temperature by adding a small amount of Rh doping ($x = 0.04$). (b) The derivative of ρ with respect to T

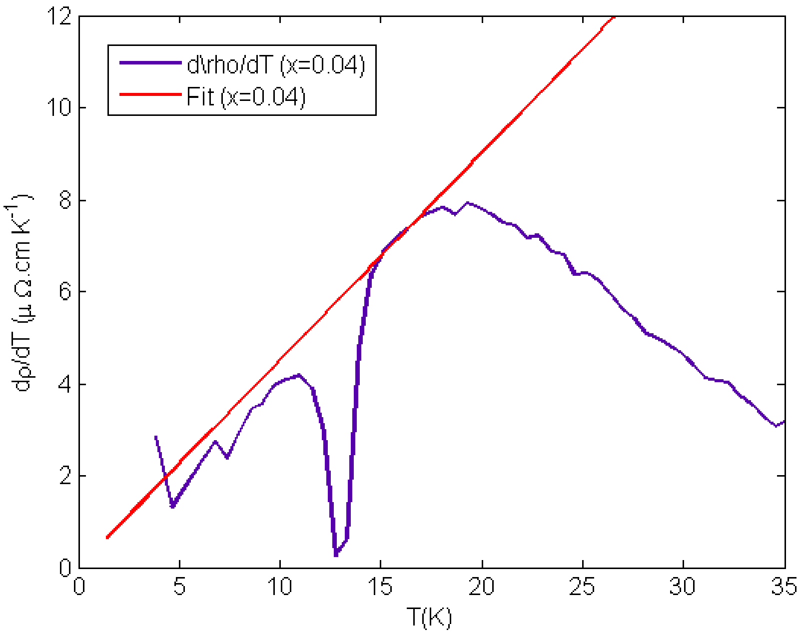

Figure 6.11: The blue curve is $d\rho/dT$ of $URu_{2-x}Rh_xSi_2$ with $x = 0.04$, the red line is the Fermi liquid fit $d\rho/dT = 2AT + \rho_0$ for the temperature range 14.35-16.35 K

Table 6.5: The fit parameters of $URu_{2-x}Rh_xSi_2$ with $x = 0.04$ in the Fermi liquid region using the formula $d\rho/dT = 2AT + B$

x	A($\mu\Omega.cmK^{-1}$)	$B(\mu\Omega.cmK^{-1})$
0.04	0.2251 ± 0.1949	0.0

6.4.2 Fermi Liquid Fit

The Fermi liquid fit of $d\rho/dT$ for $x = 0.04$ for temperature $T_{\text{HO}} + 1 \leq T \leq T_{\text{HO}} + 3$ is displayed in Figure 6.11. The fit line crosses the origin of the ρ vs. T plot as expected from table 6.5 with $B = 0$.

6.4.3 Gapped Fermi Liquid Fit

The fit of the gapped Fermi liquid equation 4.2.1 to ρ with $x = 0.04$ in the low temperature region is shown in Figure 6.12. As can be seen in table 6.6. The energy gap is for the sample with $x = 0.04$ is reduced to 65 K compared to to parent compound gap of 78 K (table 6.2) as we expected.

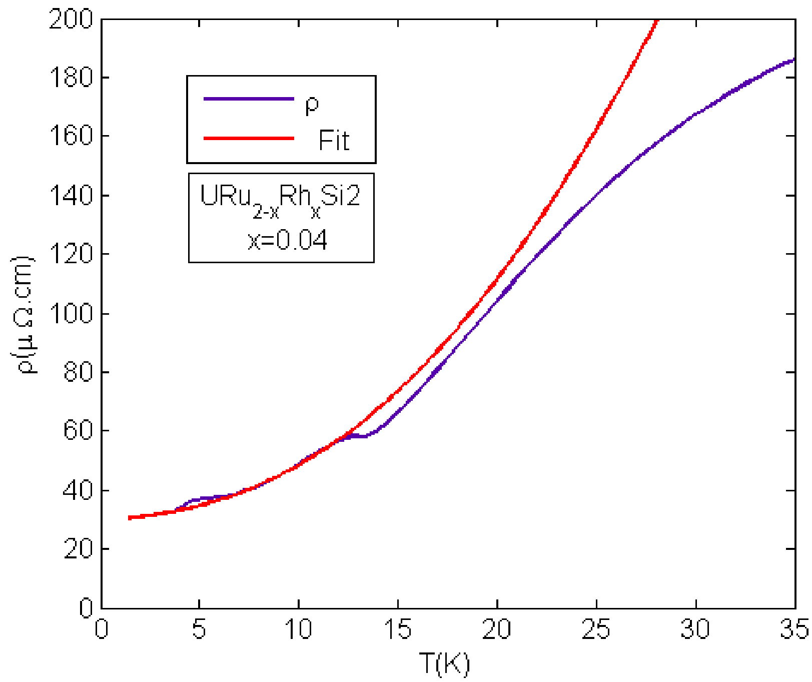

Figure 6.12: The resistivity ρ vs. T for $URu_{2-x}Rh_xSi_2$ with $x = 0.04$, the red curve is the fit in the gapped Fermi liquid region using formula 4.2.1

Table 6.6: Fit parameters of $URu_{2-x}Rh_xSi_2$ with x = 0.04 in the HO state using the formula 4.2.1

x	$\rho_0(\mu\Omega.cm)$	$B(\mu\Omega.\mathrm{cm}K^{-2})$	$A(\mu\Omega.cmK^{-2})$	$\Delta(K)$	T_{HO}
0.04	30.11 ± 0.83	150	30.11	65	13.35

6.5 Sr_2RuO_4

The crystal growth of Sr_2RuO_4 was done by Kevin Mortimer a former M. Sc candidate of Dr. Timusk's group (McMaster University) and with the technical assistance of Dr. Maeno and his group in F. The samples were wired using the four probe (Kelvin) geometry for ρ_{ab} shown in Figure 6.14 and Corbino disc geometry for ρ_c as shown as shown in inset of the left bottom panel in Figure 4.11. The main uncertainty in the absolute value of the resistivity in the Kelvin geometry comes from the distance between the voltage contacts, marked as L1, L2 and L3. We arbitrarily chose L2, the distance between the wires as a best estimate. We utilized the AC resistance bridge with lock-in detection for both ρ_{ab} and ρ_c.

6.5.1 Resistivity

The temperature dependent resistivity $\rho_{\rm ab}$ and ρ_c of our Sr_2RuO_4 sample with the lowest 3 K phase concentration is shown in Figure 6.13. As it can be seen, the resistivity is anisotropic and the sample becomes non-metallic in c direction around 140 K where the sign of $d\rho_c/dT$ changes from positive to negative.

6.5.2 Fermi Liquid fit

The resistivity data ρ_{ab} is fit from 2–20 K to the Fermi liquid equation $AT^2 + \rho_0$ as well as the equation $AT^2 + BT + \rho_0$ with a non-Fermi liquid term BT. Both fits are plotted in Figure 6.16. The coefficients of the fits with their uncertainties for the Fermi liquid case are presented in tables 6.7 for three values of L and for the non-Fermi liquid case in table 6.8 for L=0.15. As we can see the linear T contribution in the resistivity for the temperature range 4–20 K is quite small, evidence that our Sr_2RuO_4 sample shows Fermi liquid behaviour, as conventionally defined, in the range 4–20 K.

Figure 6.16 shows Sr_2RuO_4 low temperature resistivity vs. T^2. As it can be seen ρ_{ab} deviates the T-squared behaviour around $T^2 = 500$ (or T $\sim$ 22) with the Fermi liquid coefficient $A_{ab} = 7.1$ nΩcmK^{-2}. This is in agreement with Maeno *et al.*[37] who observed ab plane Fermi liquid behaviour in their Sr_2RuO_4 sample up to 25 K with $A_{ab} = 7.3$ nΩcmK^{-2}, see Figure 4.12. The

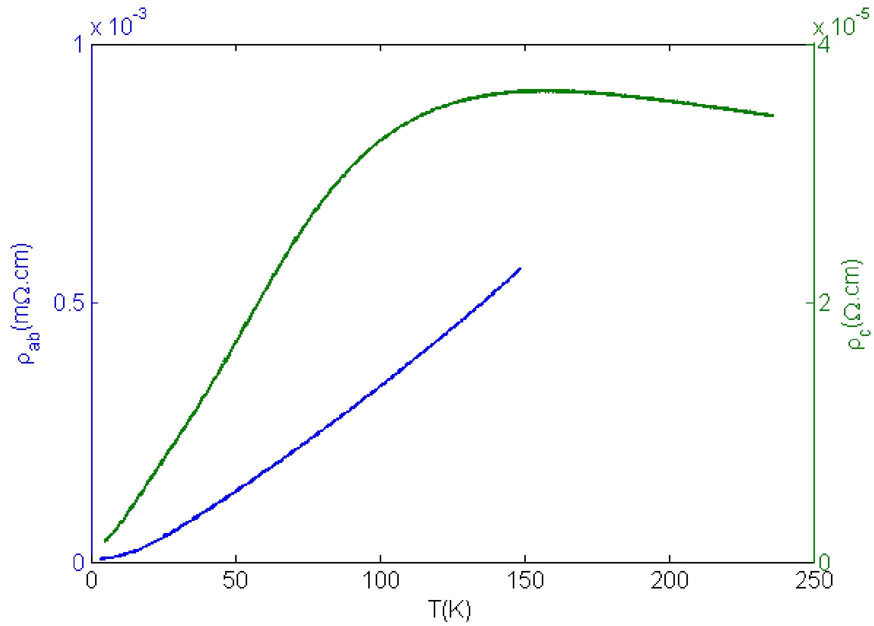

Figure 6.13: In-plane ρ_{ab} (blue curve) and interlayer ρ_c (green curve) of Sr_2RuO_4 vs. T

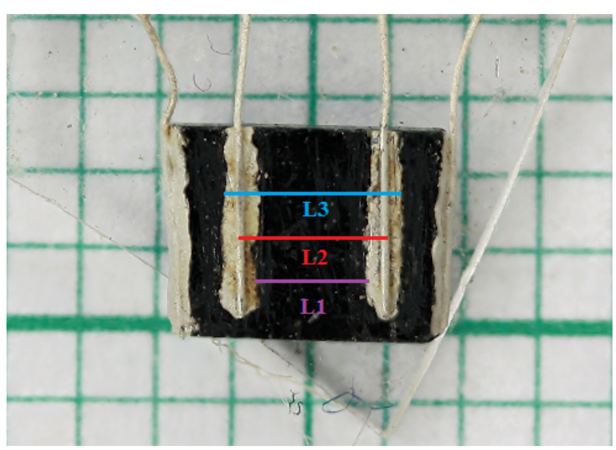

Figure 6.14: Single crystal Sr_2RuO_4 sample wired for ab-plane resistivity measurements. There is some uncertainty as to the distance between the voltage contacts marked L1, L2 and L3. We chose the average L2 for our analysis.

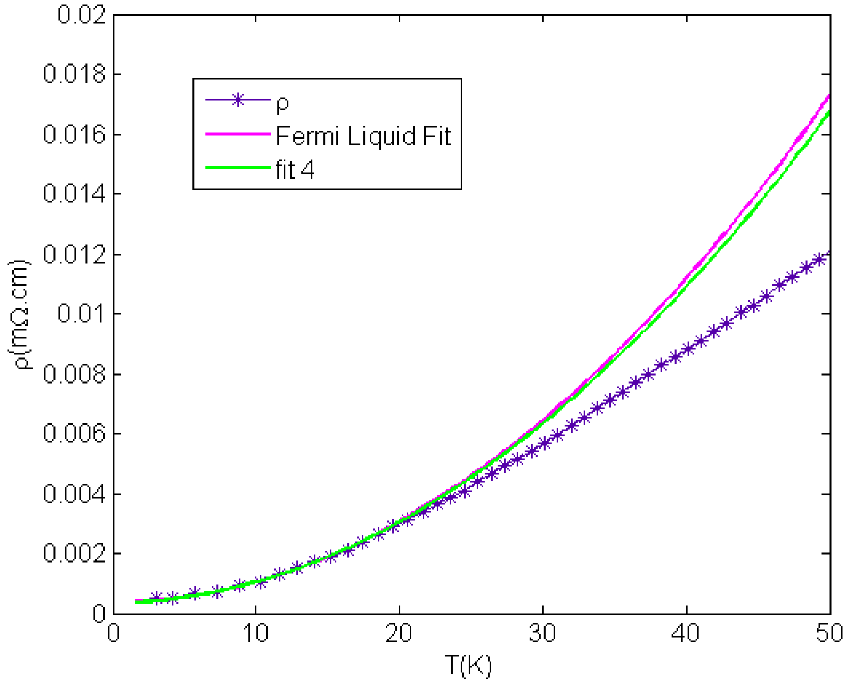

Figure 6.15: Fermi liquid fit (pink curve) for Sr_2RuO_4 using $AT^2 + \rho_0$ and fit curve $\propto T$ using $Ax^2 + Bx + \rho_0$ (green curve) which includes non Fermi liquid term $\propto T$. The fits are performed for the temperature range 2–20 K

red line is a fit to $AT^2 + \rho_0$ to the data line ρ vs.T^2 with $A = 7.11 \pm 0.5$ and $\rho_0 = 0.28 \pm 0.09$.

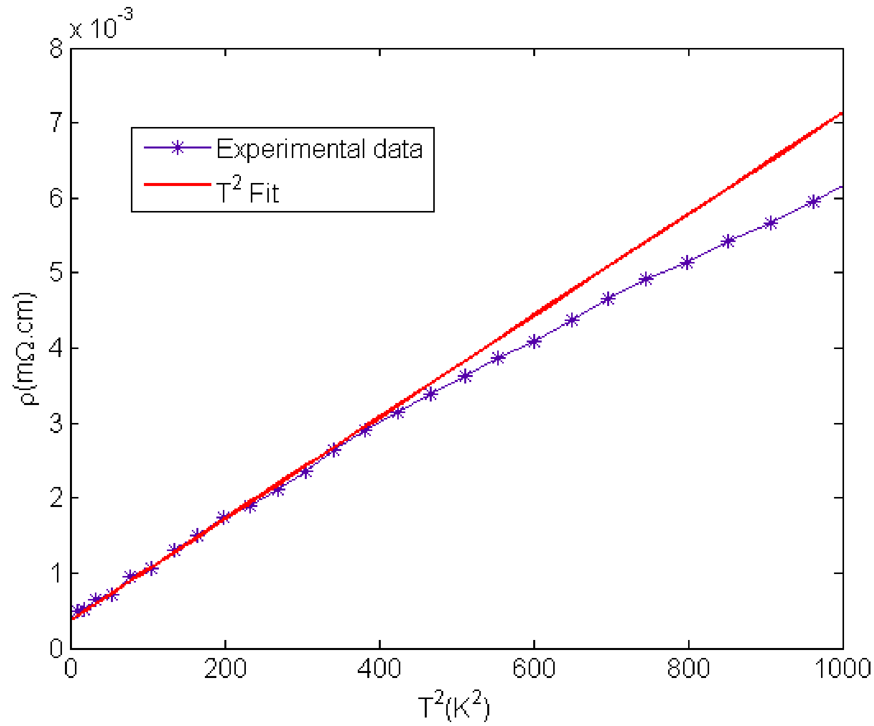

Figure 6.16: Fermi liquid fit for Sr_2RuO_4 using $AT^2 + \rho_0$. The fit is performed for the temperature range 2–20 K

Table 6.7: Fermi liquid fit parameters of Sr_2RuO_4 using $AT^2 + \rho_0$ and a non Fermi liquid fit term $\propto T$ using $AT^2 + BT + \rho_0$ for the temperature range 2-20 K are compared in this table

$AT^2 + \rho_0$	$L(cm)$	$A(n\Omega\text{cm K}^{-2})$	$\rho_0(\mu\Omega.\text{cm})$
	0.15	8.03 ± 0.26	0.45 ± 0.05
	0.18	7.1 ± 0.5	0.28 ± 0.05
	0.23	5.26 ± 0.18	0.29 ± 0.04

Table 6.8: Fermi liquid fit parameters of Sr_2RuO_4 using $Ax^2 + \rho_0$ and a non-Fermi-liquid fit term $\propto T$ using $Ax^2 + Bx + \rho_0$ for the temperature range 2-20 K are compared in this table

$AT^2 + BT + \rho_0$	$L(cm)$	$A(n\Omega.cmK^{-2})$	$B(n\Omega.cmK^{-1})$	$\rho_0(\mu\Omega.\text{cm})$
	0.18	7.1 ± 0.5	8.23 ± 42.36	0.28 ± 0.09

Chapter 7

Discussion and conclusions

The resistivity measurements on URu_2Si_2 doped with different elements (Fe, Re and Rh) are presented. All the doped URu_2Si_2 compounds show the expected Fermi liquid behaviour with $\rho(T) \propto T^2$ in the region $T_{\mathrm{HO}} + 1 < T < T_{\mathrm{HO}} + 3$ which T_{HO} is the temperature of the hidden order transition. We also studied the hidden order phase in URu_2Si_2 which is also present for this compound with different chemical substitutions. The results show that the hidden order temperature is suppressed with the addition of small amounts of Rh and Re doping and the HO order gap becomes smaller by increasing the doping concentration. However, $T_{\mathrm{HO/LMAFM}}$ was shifted to higher temperature for Fe doping and reaches its maximum at $x = 0.2$ in $URu_{2-x}Fe_xSi_2$.

In addition, by comparing the Fermi liquid fit coefficients in the tables 6.1, 6.3 and 6.5 we can conclude that all Fermi liquid coefficients A are similar within experimental errors for all the substitutions and while the hidden order state is changed dramatically by these substitutions they do not affect the Fermi liquid region just above the transition. However, for $URu_{2-x}Fe_xSi_2$ with $x = 0.3$ A is different and possible evidence that a completely new state has been entered at this doping level.

The dependence of T_{HO} of URu_2Si_2 on different doping concentrations is compared in figure 7.1. The data for other doping values other than the ones available in our lab are taken from resistivity measurements from literature. T_{HO} data for $URu_{2-x}Re_xSi_2$ $x = 0.04$ and 0.08 are from [4] resistivity data and we used $URu_{2-x}Fe_xSi_2$ with $x = 0.05$, 0.6, 0.8 and 1.0 from resistivity measurement of polycrystalline samples reported in [5]. We have also taken T_{HO} data for $URu_{2-x}Rh_xSi_2$ (except $x = 0.04$) from [10]. As we can see the

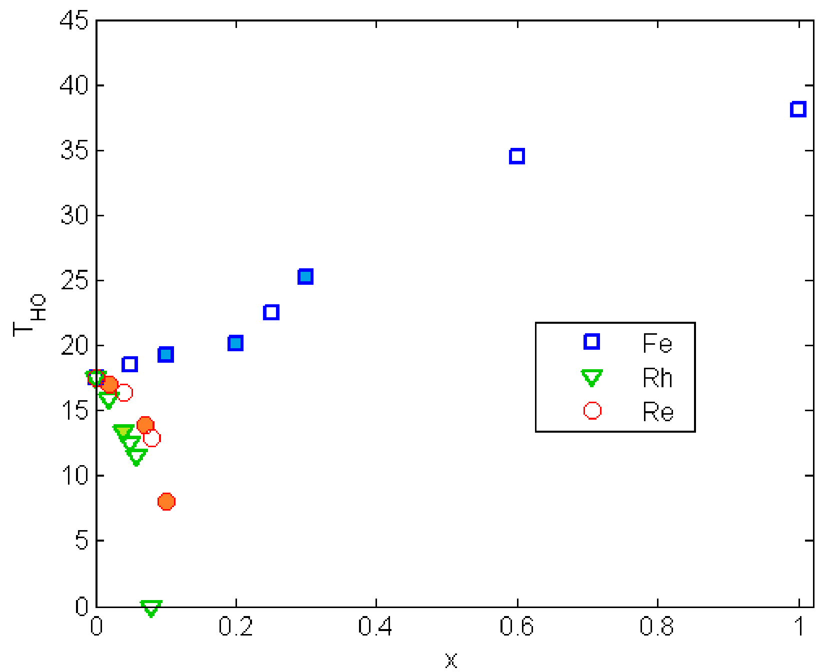

Figure 7.1: The HO temperature as a function of different doping concentrations x, The filled symbols are the resistivity data points from samples measured as described in this thesis and the filled symbols are data points from [4] (circles for Re doping) , [10] (triangle for Rh doping) and [5] (square for Fe doping)

T_{HO} shows similar profile as a function of Re and Rh dopings.

For the Sr_2RuO_4 samples we were able to verify Fermi liquid behaviour in the ab plane below 22 K with an A parameter that agreed with previous work. However in the c direction we did not see a T^2 temperature dependence in ρ_c as reported by previously by Maeno *et al.*[8]. Future work may involve remeasuring the resistivity of Sr_2RuO_4 along c-axis.

The values of the gaps and Fermi liquid parameters obtained from fits were obtained using MATLAB cftool function. Furthermore, we have successfully improved resistivity measurement techniques in our lab as it is explained in chapter 5.

Bibliography

[1] JS Hall and T Timusk. Optical study of hybridization and hidden order in URu_2Si_2 . *Philosophical Magazine*, (ahead-of-print):1–15, 2014.

[2] Urmas Nagel, Taaniel Uleksin, Toomas Rõõm, Ricardo P. S. M. Lobo, Pascal Lejay, Christopher C. Homes, Jesse S. Hall, Alison W. Kinross, Sarah K. Purdy, Tim Munsie, Travis J. Williams, Graeme M. Luke, and Thomas Timusk. Optical spectroscopy shows that the normal state of URu_2Si_2 is an anomalous Fermi liquid. *Proceedings of the National Academy of Sciences*, 109(47):19161–19165, 2012.

[3] Tatsuma D. Matsuda, Elena Hassinger, Dai Aoki, Valentin Taufour, Georg Knebel, Naoyuki Tateiwa, Etsuji Yamamoto, Yoshinori Haga, Yoshichika Ōnuki, Zachary Fisk, et al. Details of sample dependence and transport properties of URu_2Si_2 . *Journal of the Physical Society of Japan*, 80(11), 2011.

[4] Nicholas P Butch and M Brian Maple. The suppression of hidden order and the onset of ferromagnetism in URu_2Si_2 via re substitution. *Journal of Physics: Condensed Matter*, 22(16):164204, 2010.

[5] N Kanchanavatee, M Janoschek, RE Baumbach, JJ Hamlin, DA Zocco, K Huang, and MB Maple. Twofold enhancement of the hidden-order/large-moment antiferromagnetic phase boundary in the URu_2Si_2 system. *Physical Review B*, 84(24):245122, 2011.

[6] Y Dalichaouch, MB Maple, JW Chen, T Kohara, C Rossel, MS Torikachvili, and AL Giorgi. Effect of transition-metal substitutions on competing electronic transitions in the heavy-electron compound URu_2Si_2 . *Physical Review B*, 41(4):1829, 1990.

[7] Y. Maeno, H. Hashimoto, K. Yoshida, S. Nishizaki, T. Fujita, J. G. Bednorz, and F. Lichtenberg. Superconductivity in a layered perovskite without copper. *Nature*, 372:532–534, December 1994.

[8] Y Maeno, S Nishizaki, K Yoshida, S Ikeda, and T Fujita. Normal-state and superconducting properties of Sr_2RuO_4 . *Journal of low temperature physics*, 105(5-6):1577–1586, 1996.

[9] I. Nagai, N. Shirakawa, N. Umeyama, and S.-I. Ikeda. Quasi-Two-Dimensional Fermi-Liquid State in Sr_2RhO_{4-d}. *Journal of the Physical Society of Japan*, 79(11):114719, nov 2010.

[10] Makoto Yokoyama, Hiroshi Amitsuka, Seiichiroh Itoh, Ikuto Kawasaki, Kenichi Tenya, and Hideki Yoshizawa. Neutron scattering study on competition between hidden order and antiferromagnetism in $U(Ru_{1-x}Rh_x)2Si_2$ (x 0.05). *Journal of the Physical Society of Japan*, 73(3):545–548, 2004.

[11] Radii Nikolaevich Gurzhi. Mutual electron correlations in metal optics. *Soviet Physics Journal of Experimental and Theoretical Physics*, 35:673–675, 1959.

[12] Dmitrii L. Maslov and Andrey V. Chubukov. First-matsubara-frequency rule in a fermi liquid. ii. optical conductivity and comparison to experiment. *Phys. Rev. B*, 86:155137, Oct 2012.

[13] K Andres, JE Graebner, and HR Ott. 4 f-virtual-bound-state formation in $CeAl_3$ at low temperatures. *Physical Review Letters*, 35(26):1779, 1975.

[14] Piers Coleman. *Heavy fermions: Electrons at the edge of magnetism*. Wiley Online Library, 2007.

[15] Jun Kondo. Resistance minimum in dilute magnetic alloys. *Progress of theoretical physics*, 32(1):37–49, 1964.

[16] Alexander Cyril Hewson. *The Kondo problem to heavy fermions*. Number 2. Cambridge University Press, 1997.

[17] Philip Warren Anderson. Localized magnetic states in metals. *Physical Review*, 124(1):41, 1961.

[18] JR Schrieffer and PA Wolff. Relation between the anderson and kondo hamiltonians. *Physical Review*, 149(2):491, 1966.

[19] S Doniach. The kondo lattice and weak antiferromagnetism. *Physica B+ C*, 91:231–234, 1977.

[20] GR Stewart, Z Fisk, JO Willis, and JL Smith. Possibility of coexistence of bulk superconductivity and spin fluctuations in UPt_3. *Physical Review Letters*, 52(8):679, 1984.

[21] HR Ott, H Rudigier, Z Fisk, and JL Smith. UBe_{13}: An unconventional actinide superconductor. *Physical Review Letters*, 50(20):1595, 1983.

[22] JA Mydosh and Peter M Oppeneer. Colloquium: Hidden order, superconductivity, and magnetism: The unsolved case of URu_2Si_2 . *Reviews of Modern Physics*, 83(4):1301, 2011.

[23] TTM Palstra, AA Menovsky, J Van den Berg, AJ Dirkmaat, PH Kes, GJ Nieuwenhuys, and JA Mydosh. Superconducting and magnetic transitions in the heavy-fermion system URu_2Si_2 . *Physical Review Letters*, 55(24):2727, 1985.

[24] Y Kasahara, T Iwasawa, H Shishido, T Shibauchi, K Behnia, Y Haga, TD Matsuda, Y Onuki, M Sigrist, and Y Matsuda. Exotic superconducting properties in the electron-hole-compensated heavy-fermion semimetal URu_2Si_2 . *Physical Review Letters*, 99(11):116402, 2007.

[25] W Schlabitz, J Baumann, B Pollit, U Rauchschwalbe, HM Mayer, U Ahlheim, and CD Bredl. Superconductivity and magnetic order in a strongly interacting fermi-system: URu_2Si_2 . *Zeitschrift für Physik B Condensed Matter*, 62(2):171–177, 1986.

[26] MB Maple, JW Chen, Y Dalichaouch, T Kohara, C Rossel, MS Torikachvili, MW McElfresh, and JD Thompson. Partially gapped fermi surface in the heavy-electron superconductor URu_2Si_2 . *Physical Review Letters*, 56(2):185, 1986.

[27] Andrew R Schmidt, Mohammad H Hamidian, Peter Wahl, Focko Meier, Alexander V Balatsky, JD Garrett, Travis J Williams, Graeme M Luke,

and JC Davis. Imaging the fano lattice to hidden order transition in URu_2Si_2 . *Nature*, 465(7298):570–576, 2010.

[28] RA Fisher, S Kim, Y Wu, NE Phillips, MW McElfresh, MS Torikachvili, and MB Maple. Specific heat of URu_2Si_2 : Effect of pressure and magnetic field on the magnetic and superconducting transitions. *Physica B: Condensed Matter*, 163(1):419–423, 1990.

[29] MW McElfresh, JD Thompson, JO Willis, MB Maple, T Kohara, and MS Torikachvili. Effect of pressure on competing electronic correlations in the heavy-electron system URu_2Si_2 . *Physical Review B*, 35(1):43, 1987.

[30] E Hassinger, TD Matsuda, G Knebel, V Taufour, D Aoki, and J Flouquet. Inelastic contribution of the resistivity in the hidden order in URu_2Si_2 . In *Journal of Physics: Conference Series*, volume 273, page 012031. IOP Publishing, 2011.

[31] Gaku Motoyama, Takashi Nishioka, and Noriaki K Sato. Phase transition between hidden and antiferromagnetic order in URu_2Si_2 . *Physical Review Letters*, 90(16):166402, 2003.

[32] E. Hassinger, G. Knebel, T. D. Matsuda, D. Aoki, V. Taufour, and J. Flouquet. Similarity of the fermi surface in the hidden order state and in the antiferromagnetic state of uru_2si_2. *Phys. Rev. Lett.*, 105:216409, Nov 2010.

[33] F. Lichtenberg, A. Catana, J. Mannhart, and D. G. Schlom. Sr_2RuO_4: A metallic substrate for the epitaxial growth of $YBa_2Cu_3O_{7-d}$. *Applied Physics Letters*, 60:1138–1140, 1992.

[34] Tetsuo Shimura, Mitsuru Itoh, and Tetsurō Nakamura. Novel two-dimensional conductor Sr_2RhO_4 . *Journal of Solid State Chemistry*, 98(1):198–200, 1992.

[35] LJ Van der Pauw. A method of measuring the resistivity and hall coefficient on lamellae of arbitrary shape. *Philips technical review*, 20(8):220–224, 1958.

[36] J. Ekin. *Experimental Techniques for Low-Temperature Measurements : Cryostat Design, Material Properties and Superconductor Critical-Current Testing.* OUP Oxford, 2006.

[37] Yoshiteru Maeno, Koji Yoshida, Hiroaki Hashimoto, Shuji Nishizaki, Shin-ichi Ikeda, Minoru Nohara, Toshizo Fujita, Andrew P Mackenzie, Nigel E Hussey, J Georg Bednorz, et al. Two-dimensional fermi liquid behavior of the superconductor Sr_2RuO_4 . *Journal of the Physical Society of Japan*, 66(5):1405–1408, 1997.

Appendices

Appendix A

MATLAB codes

A.1 Calculating $d\rho/dT$ and plotting

```
rhofname='filename.dat';

%T temprature and R resistance collected using 4-point measurement
{time,T, H,Freq,I,V,Z1,R]=textread(rhofname,'%f %f %f %f
%f %f %f %f','headerlines',2);


Rho=10^3.*R.*a*.b./L;    %[mohm.cm] a,b and L: sample dimensions in cm

%derivative-5 point center
Rho_zero=Rho(1);
dRho=Rho;

for it=3:numel(Rho)-3
     dRho(it)=(Rho(it-2)-8.*Rho(it-1)
    +8.*Rho(it+1)-Rho(it+2))./(12.*(T(it+1)-T(it)));
end

plot(T(:),Rho(:), 'r'); hold on;
plot(T(:),10.*dRho(:), 'b');
```

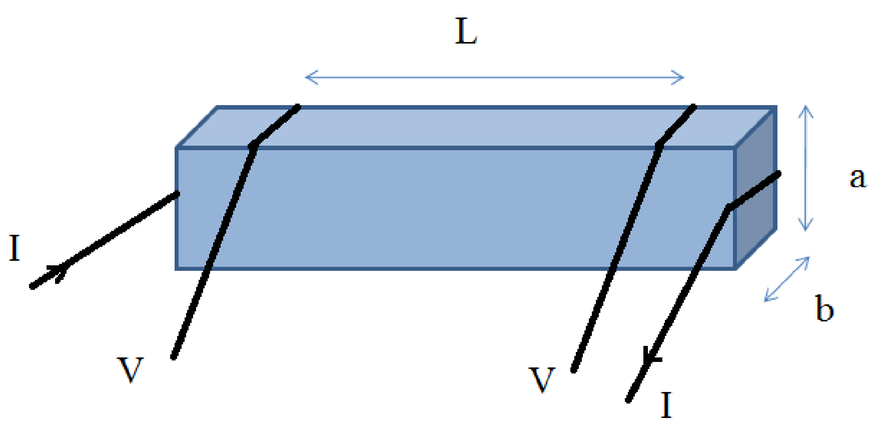

Figure A.1: Four point resistance geometry sample dimensions.